Study of Light Λ- and $\Lambda\Lambda$-Hypernuclei with the Stochastic Variational Method and Effective ΛN Potentials

Hidekatsu NEMURA[1], Yasuyuki SUZUKI[2], Yoshikazu FUJIWARA[3] and Choki NAKAMOTO[4]
[1] *Graduate School of Science and Technology, Niigata University, Niigata 950-2181, Japan*
[2] *Department of Physics, Niigata University, Niigata 950-2181, Japan*
[3] *Department of Physics, Kyoto University, Kyoto 606-8502, Japan*
[4] *Suzuka National College of Technology, Suzuka, Mie 510-0294, Japan*
(February 9, 2008)

We first determine the ΛN S-wave phase shifts so as to reproduce the experimental Λ separation energies of $A = 3$, 4 Λ-hypernuclei (${}^{3}_{\Lambda}$H, ${}^{4}_{\Lambda}$H, ${}^{4}_{\Lambda}$He, ${}^{4}_{\Lambda}$H*, and ${}^{4}_{\Lambda}$He*), and then construct three phase-equivalent ΛN potentials with different central repulsion. By the stochastic variational method with correlated Gaussian basis we perform an extensive calculation of *ab initio* type for the hypernuclei of up to A=6. The binding energies and the sizes of the Λ-hypernuclei are very insensitive to the type of the phase-equivalent ΛN potentials. We use two different $\Lambda\Lambda$ potentials which both reproduce $\Delta B_{\Lambda\Lambda}({}^{6}_{\Lambda\Lambda}\mathrm{He})$ reasonably well. Any combination of these ΛN and $\Lambda\Lambda$ potentials predicts hitherto undiscovered particle-stable bound states, ${}^{4}_{\Lambda\Lambda}$H, ${}^{5}_{\Lambda\Lambda}$H and ${}^{5}_{\Lambda\Lambda}$He: Predicted values of $B_{\Lambda\Lambda}$ are about 0.4, 5.5 and 6.3 MeV, respectively. The binding energy of ${}^{4}_{\Lambda\Lambda}$H is so small that its possibility crucially depends on the strength of the $\Lambda\Lambda$ interaction. The binding energies of both ${}^{5}_{\Lambda}$He and ${}^{6}_{\Lambda\Lambda}$He are calculated to be strongly overbound compared to experiment. In relation to this well-known anomaly we examine the effect of the quark substructure of N and Λ on their binding energies. The effect is negligible if the baryon size in which three quarks are confined is smaller than 0.6 fm, but becomes appreciable, particularly in ${}^{6}_{\Lambda\Lambda}$He, if the size is taken to be as large as 0.7 fm. We discuss the extent to which the nucleon subsystem in the hypernuclei changes by the addition of Λ particles. The charge symmetry breaking of the ΛN potential is phenomenologically determined and concluded to be weakly spin-dependent.

I. INTRODUCTION

Strangeness or hypernuclear physics has been attracting increasing interest in recent years [1]. Experimental progress on both a production of hypernuclei with strangeness $S = -1$ and -2 and an analysis of their decay modes will bring rich information on the baryon dynamics involving strange particles. It may be particularly interesting to make clear to what extent the properties of a strange particle in nuclear medium change from those in a free space.

The knowledge of the hyperon-nucleon (YN) interaction is crucially important for a further development of the hypernuclear physics. Because of the limited data on Λ-nucleon (ΛN) scatterings, no reliable phase shift analysis has been performed yet. Even the $\boldsymbol{\sigma}_\Lambda \cdot \boldsymbol{\sigma}_N$ part of the ΛN interaction has not been determined precisely. Though one-boson-exchange (OBE) models [2,3] or quark cluster models [4] for YN interactions have produced useful results on the interactions and have shown some predictive power, the behavior of the ${}^1S_0$ or the ${}^3S_1$ phase shift is not always the same in these models. At present it is not possible to pin down realistic potentials which can be used in *ab initio* hypernuclear structure calculations.

In view of this circumstance, hypernuclear spectroscopic study will be aided by modeling effective ΛN and $\Lambda\Lambda$ potentials. One may determine the potentials phenomenologically so as to reproduce the binding energies of light Λ- and $\Lambda\Lambda$-hypernuclei before theoretically sound, realistic potentials become available. In fact, the early work [5] performed more than a quarter of a century ago with the effective ΛN potential demonstrated that the observed binding energy of ${}^{5}_{\Lambda}$He is anomalously small. This problem still remains an enigma [6] despite of several attempts at resolving this anomaly by the mechanism of e.g., tensor forces [7] or ΛN-ΣN couplings. Since the excited states of the $A = 4$ isodoublets (${}^{4}_{\Lambda}$H* and ${}^{4}_{\Lambda}$He*) had not been well established in those days, it will be worthwhile to redetermine effective ΛN potentials which include the charge symmetry breaking (CSB) effect.

The information on effective ΛN interactions becomes available together with the progress in technique for a precise solution of few-body systems. A detailed, systematic analysis of the binding mechanism of light hypernuclei may make it possible to determine the S-wave strength of the ΛN interaction. As is well-known, the binding energies of the $A = 3$, 4 hypernuclei strongly depend on the relative strength of attraction between ${}^1S_0$ and ${}^3S_1$ states. If the ${}^1S_0$ attraction is only slightly stronger than the ${}^3S_1$ one as in the case of the Nijmegen model F [3](NF) or Dalitz *et al.* [5] potential, we would have not only the ground state ($J^\pi = \frac{1}{2}^+$) but also a particle-stable excited state ($J^\pi = \frac{3}{2}^+$)

of ${}^{3}_{\Lambda}$H. The latter has not experimentally been confirmed yet. This type of potentials predicts a too small energy difference of the two states (0^+ and 1^+) for the $A = 4$ isodoublets. On the contrary, one of the versions of the quark cluster model, FSS [4], gives a very strong attraction in ${}^1S_0$ and leads to the overbinding of ${}^{3}_{\Lambda}$H as well as a too large energy difference for the two states in the $A = 4$ system. Recently the simplest three baryon system YNN with $S = -1$ has been studied [8] in the Faddeev method, which shows that only the Nijmegen soft core (NSC89) potential [9], among others, reproduces the experimental $B_\Lambda({}^{3}_{\Lambda}\mathrm{H})$ value. The work has also shown clearly the importance for the ΛN-ΣN conversion and its ${}^3S_1$-${}^3D_1$ tensor coupling for producing the bound state of ${}^{3}_{\Lambda}$H. The new version of the Nijmegen soft core model (NSC97 [10]) has been constructed on the basis of these theoretical developments.

The purpose of the present study is threefold: First we determine phenomenologically such effective ΛN central potentials that reproduce the binding energies of s-shell hypernuclei (${}^{3}_{\Lambda}$H, ${}^{4}_{\Lambda}$H, ${}^{4}_{\Lambda}$He, ${}^{4}_{\Lambda}$H*, ${}^{4}_{\Lambda}$He*). Secondly, we explore the possibility of whether $\Lambda\Lambda$-hypernuclei with $A = 4$, 5 form bound states or not by employing the available $\Lambda\Lambda$ potentials. This will be useful for experimental search for these $\Lambda\Lambda$-hypernuclei. A confirmation of the lightest $\Lambda\Lambda$-hypernuclei as well as the H-particle will give us useful information on the strength of the $\Lambda\Lambda$ interaction. Thirdly, we investigate to what extent the quark substructure of the baryons plays a role in reducing the Λ separation energy of the hypernuclei with $A \geq 5$.

The third point mentioned above is expected to reveal, through hypernuclear studies, a unique role of the quark substructure of baryons. The binding energies of the Λ-hypernuclei have so far been calculated on the premise that they ought to be understood provided two- and three-body baryonic interactions are precisely known. This seems quite natural because the Λ-particle can be distinguished from the nucleon at the baryon level. However, if we take into account the quark substructure of the baryon, the Pauli principle acting at the underlying quark level produces certain constraints on the dynamical motion of the hypernuclear system, because both N and Λ contain u and d quarks. This quark Pauli effect has recently been studied in Refs. [11] and [12] as a function of the baryon size b in which three quarks are confined. The reduction of the binding energy of ${}^{5}_{\Lambda}$He and ${}^{6}_{\Lambda\Lambda}$He is found to occur at $b \geq 0.6$ fm.

It is of vital importance for achieving the above objectives that we can obtain a precise solution of few-body problems. A fair description of the correlated motion is an essential ingredient to get accurate solutions. As tested in a variety of examples in atomic and nuclear few-body problems [13,14], the correlated Gaussian (CG) basis leads to a virtually exact solution. This basis explicitly describes the correlated motion of the constituent particles, and its simple form makes it possible to obtain matrix elements analytically. We therefore use a variational trial function given as a combination of the CGs, and increase the basis dimension one by one till a practical convergence is attained. The optimization of the nonlinear parameters contained in the basis functions is performed by selecting the best among a number of candidates randomly chosen. This gambling procedure is called the stochastic variational method (SVM) [13–15].

We will focus on central components, both spin-independent and spin-dependent, of the potential, so the systems considered here are limited to those hypernuclei whose total orbital angular momentum is well approximated by $L = 0$. We presume that the effects of tensor forces, three-body forces and Λ-Σ conversion etc. are effectively replaced by a central force in fitting the binding energies of the s-shell hypernuclei. The hypernuclei with $A \leq 6$ are treated, without any compromise, as an A-baryon system and their energies are calculated by fully taking into account the dynamics of the constituent baryons.

We present in sect. 2 the formalism of the present study. The effective ΛN potential is determined in subsect. 2.1 by starting from potentials phase equivalent to the Nijmegen model [3] or the quark cluster model [4]. The $\Lambda\Lambda$ potentials used in the present study are briefly mentioned in this subsection. The variational trial function with the CGs is given in subsect. 2.2. The optimization of the parameters of the trial function is carried out as described in subsect. 2.3. Results of calculation are given in sect. 3. The Λ-hypernuclei with $A \leq 5$ and $\Lambda\Lambda$-hypernuclei with $A \leq 6$ are discussed in subsects. 3.1 and 3.2, respectively. The Λ density distribution and the $\Lambda\Lambda$-correlation function are calculated in subsect. 3.3 in order to exhibit the structure of the hypernuclei. We also analyze the extent to which the nuclear core changes by adding Λ particles. The CSB term of the ΛN potential is discussed in subsect. 3.4 and its strength is determined phenomenologically. We consider in subsect. 4.1 a special configuration constrained by the Pauli principle at the quark level. Results for ${}^{5}_{\Lambda}$He, ${}^{5}_{\Lambda}$H and ${}^{6}_{\Lambda\Lambda}$He are presented in subsect. 4.2. Summary is given in sect. 5. Some formulas for the matrix elements of the CGs are collected in appendix.

II. THE FORMALISM

A. Potentials

As mentioned in the introduction, our aim in this subsection is to determine effective ΛN central forces that presumably include various effects such as the tensor force, the three-body force and so on. The Minnesota potential [16] is such a type of central potential widely employed as the NN potential. The Minnesota potential is given in a form

$$V = \left\{ V_R + \frac{1}{2}(1+P^\sigma)V_t + \frac{1}{2}(1-P^\sigma)V_s \right\} \left\{ \frac{1}{2}u + \frac{1}{2}(2-u)P^r \right\}, \tag{1}$$
$$V_R = V_{0R}\mathrm{e}^{-\kappa_R r^2}, \quad V_t = -V_{0t}\mathrm{e}^{-\kappa_t r^2}, \quad V_s = -V_{0s}\mathrm{e}^{-\kappa_s r^2},$$

where P^σ and P^r are spin- and space-exchange operators, respectively. An adjustable parameter u determines the strength of odd partial-waves between the baryons.

(i) NN potential

The parameters of the Minnesota potential were determined so as to reproduce the low-energy NN scattering data. This potential is adopted as the NN potential in what follows. One nice, noteworthy point is that the Minnesota potential reproduces reasonably well both the binding energies and sizes of few-nucleon systems such as ^{2}H, ^{3}H, ^{3}He and ^{4}He [13]. This is a necessary condition for the present purpose. Results of our calculation are insensitive to the choice of u because even partial-waves are predominant components, so u may be set to unity. The Coulomb potential is included in the present calculation.

(ii) ΛN potential

Due to the experimental limitation of Λp scattering, the ΛN interaction is rather poorly known. Though various versions of a model description for the ΛN interaction can reproduce the existing Λp scattering data, the properties given by them are different from each other. For example, the $^1S_0$ and $^3S_1$ phase shifts scatter depending on the model, though they are quite important for binding the Λ-hypernuclei.

The relative importance of $^1S_0$ and $^3S_1$ ΛN potentials may be estimated in a simple *core nucleus*+Λ model for the s-shell Λ hypernuclei [5]. The Λ separation energy, B_Λ, may be estimated by $B_\Lambda = -(A-1)\langle V_R\rangle - N_s\langle V_s\rangle - N_t\langle V_t\rangle$ when the kinetic energy contribution is neglected, where $\langle V_s\rangle$, for example, is the average of the ΛN potential matrix elements in singlet states, and the number $N_s(N_t)$ of ΛN pairs in the singlet (triplet) state is obtained by

$$\begin{pmatrix} N_t \\ N_s \end{pmatrix} = \left\langle \sum_{i=1}^{A-1} \frac{1}{2}(1 \pm P^\sigma_{i\Lambda}) \right\rangle = \frac{A-1}{2} \pm \left(\frac{A-1}{4} + \langle \boldsymbol{J}_c \cdot \boldsymbol{S}_\Lambda \rangle \right), \tag{2}$$

where $\boldsymbol{J}_c$ is the spin of the core nucleus, $\boldsymbol{S}_\Lambda$ is the spin of Λ, and the total angular momentum $\boldsymbol{J}$ of the s-shell Λ-hypernuclei is $\boldsymbol{J}=\boldsymbol{J}_c+\boldsymbol{S}_\Lambda$. Table I lists the number of pairs obtained by assuming that the spin of the nuclear core remains unchanged by the addition of Λ. The fact that the ground state spin of ${}^3_\Lambda$H is $J=\frac{1}{2}$ but not $J=\frac{3}{2}$ indicates that the $^1S_0$ potential is more attractive than the $^3S_1$ potential. This conclusion is also consistent with the fact that the ground states of the $A=4$ hypernuclei, ${}^4_\Lambda$H and ${}^4_\Lambda$He, have $J=0$ instead of $J=1$. The energy splitting of the two states with different J values is expected to give us some information on the spin-dependent part of the ΛN interaction. The above argument is qualitative. It is noted that in reality the dynamical effect of the ΛN-ΣN coupling modifies the contribution of the $^1S_0$ and $^3S_1$-$^3D_1$ ΛN interaction components from the value of Table I, as shown in Ref. [8] for the $A=3$, $J=\frac{1}{2}$ system.

We adopt, for the ΛN potential, the same form (1) as the NN potential. This ansatz is reasonable because of the similarity between NN and ΛN, which is expected from the flavor $SU(3)$ symmetry. In particular the $^1S_0$ ΛN channel is dominated by $(\lambda\mu) = (22)$ $SU(3)$ symmetry [17], which is exactly the symmetry of the $^1S_0$ NN channel. The CSB term of the ΛN potential will be considered in subsect. 3.4.

The potential depth and range were determined as follows. First we determined the potential parameters so as to reproduce the ΛN S-wave phase shifts predicted by the NF [3] or the FSS [4] model (see Fig. 1). Then the binding energies of the $A=3$, 4 Λ-hypernuclei were calculated by using this phase equivalent potential. By taking a suitable combination of these two different potentials we attempted to reproduce the binding energy data. The S-wave phase shifts calculated by the resultant potential was then fitted by a three-range Gaussian potential (1). Of course the last procedure does not lead to a unique parameter set. In fact we could find a set of the parameters for a given value V_{0R} of the repulsive part. Three sets of parameters determined in this way are listed in Table II.

The potentials of sets A and B, used in Refs. [11] and [12], have a moderate height of the central repulsion, while the repulsion of the set C potential is chosen to be exceedingly large. The potentials of quite different core heights are constructed in order to examine the extent to which the binding energy and the quark Pauli effect depend

on the potential shape, that is the dependence of the energy on off-shell properties of the potential. Though the potential shapes are different from each other as shown in Fig. 2, they give practically the same low-energy scattering parameters, i.e., the phase shifts, the scattering lengths and the effective ranges. The S-wave phase shifts calculated by these effective potentials are compared in Fig. 1 to those by the NF and FSS models. The $^1S_0$ and $^3S_1$ phase shifts predicted by the effective potentials grow up to 32 and 19 degrees, respectively. This difference in the phase shifts is necessary to explain the energy splitting of the 0^+ and 1^+ states of the A=4 systems. The ΛN potential used by Dalitz *et al.* [5] gives similar phase shifts between $^1S_0$ and $^3S_1$ states.

The parameter u of the ΛN potential is rather insensitive to the binding energy data of the $A=3-5$ hypernuclei because the ΛN S-waves play a predominant role. This parameter was determined to be $u=1.5$ so as to fit the forward and backward ratio of the Λp scattering data [18,19], as was done by Dalitz *et al* [5]. The sensitivity to u of the ratio is shown in Fig. 3.

The total cross section for Λp scattering is shown in Fig. 4. Our parameter set underestimates the experimental data in low-energy region. Some improvement is obtained by introducing the CSB term, as we will discuss in subsect. 3.4.

Miyagawa *et al.* [8] have reported that the Nijmegen model NSC89 [9] reproduces the binding energy of ${}^{3}_{\Lambda}$H. According to their analysis, the $^1S_0$ attraction of the ΛN interaction is quite important for reproducing the binding energy of ${}^{3}_{\Lambda}$H. The scattering lengths of the model NSC89 are $a_s=-2.78$ fm and $a_t=-1.41$ fm in a charge symmetric case. The corresponding lengths predicted by our effective potentials agree with those values within 15 %; $a_s=-2.52$ fm and $a_t=-1.20$ fm.

(iii) $\Lambda\Lambda$ potential

Since there are no data for $\Lambda\Lambda$ scatterings, $\Lambda\Lambda$ potentials are derived theoretically and the soundness of the potential may be tested against the binding energy data of the $\Lambda\Lambda$-hypernuclei. In the flavor $SU(3)$ symmetry the dominant component of the $\Lambda\Lambda$ channel is again $(\lambda\mu)=(22)$ [17] but its probability is reduced to about 70 %. Only three $\Lambda\Lambda$-hypernuclei have so far been confirmed experimentally. The binding energies of these nuclei seem to imply that the $\Lambda\Lambda$ interaction is weakly attractive. The strength of the $\Lambda\Lambda$ attraction in the $\Lambda\Lambda$-hypernuclei may be estimated by the $\Delta B_{\Lambda\Lambda}$ value:

$$\begin{aligned}\Delta B_{\Lambda\Lambda}({}^{A}_{\Lambda\Lambda}\mathrm{X}) &= B_{\Lambda}({}^{A}_{\Lambda\Lambda}\mathrm{X}) - B_{\Lambda}({}^{A-1}_{\Lambda}\mathrm{X}) \\ &= B_{\Lambda\Lambda}({}^{A}_{\Lambda\Lambda}\mathrm{X}) - 2B_{\Lambda}({}^{A-1}_{\Lambda}\mathrm{X}). \end{aligned} \tag{3}$$

The experimental $\Delta B_{\Lambda\Lambda}$ values are $\Delta B_{\Lambda\Lambda}({}^{6}_{\Lambda\Lambda}\mathrm{He}) = 4.7\pm0.6$ MeV [22], $\Delta B_{\Lambda\Lambda}({}^{10}_{\Lambda\Lambda}\mathrm{Be}) = 4.3\pm0.4$ MeV [23] and $\Delta B_{\Lambda\Lambda}({}^{13}_{\Lambda\Lambda}\mathrm{B}) = 4.8\pm0.7$ MeV [24]. (Another interpretation of the last data implies $\Delta B_{\Lambda\Lambda}({}^{10}_{\Lambda\Lambda}\mathrm{B}) = -4.9\pm0.7$ MeV.) We note in passing that the corresponding value for the nn attraction may be estimated as

$$\Delta B_{nn} = B({}^{3}\mathrm{H}) - 2B({}^{2}\mathrm{H}) \cong 4.0\mathrm{MeV},$$

which is in contradiction with the expectation that the nn interaction is more attractive than the $\Lambda\Lambda$ interaction. This contradiction is probably because both ^{3}H and ^{2}H are rather weakly coupled systems.

We use two types of $\Lambda\Lambda$ potentials which predict weak attraction: One is the potential, denoted OBE-sim [25], which is phase equivalent to the Nijmegen model D (ND) potential [2], and another is the potential, denoted FSS-sim, which is phase equivalent to the quark cluster model FSS [26]. See Table II for the potential parameters of FSS-sim. The scattering lengths and effective ranges predicted by these $\Lambda\Lambda$ potentials are

$$\begin{aligned} a_s &= -2.80\mathrm{fm}, \quad r_s = 2.81\mathrm{fm} \quad \text{(OBE-sim)} \\ a_s &= -3.01\mathrm{fm}, \quad r_s = 2.16\mathrm{fm} \quad \text{(FSS-sim)} \\ a_s &= -3.01\mathrm{fm}, \quad r_s = 2.14\mathrm{fm} \quad \text{(FSS)}. \end{aligned}$$

Figure 5 compares the $^1S_0$ phase shifts calculated by the three models, and exhibits the potential shapes of the OBE-sim and FSS-sim models.

B. Variational Trial Functions

The Hamiltonian H of the system comprising nucleons and Λ particles is given by

$$H = T + V = \sum_{i=1}^{A} \frac{\boldsymbol{p}_i^2}{2m_i} - T_{cm} + V^{(NN)} + V^{(\Lambda N)} + V^{(\Lambda\Lambda)} + V^{(C)}, \tag{4}$$

where $V^{(C)}$ is the Coulomb potential between the protons. The mass of N is taken as $\hbar^2/m_N = 41.47$ MeV·fm^2 and the mass of Λ is set to be $m_\Lambda/m_N = 1.18826$. In the present study, we calculate the binding energies of various systems up to $A=6$ in a complete A-body treatment. The trial function for the eigenfunction of H is given by a combination of basis functions:

$$\Psi_{JMTM_T} = \sum_{k=1}^{K} c_k \varphi_k, \tag{5}$$

where the basis function φ_k is given by

$$\varphi_k = \mathcal{A}\{G(\boldsymbol{x}, A_k)\chi_{kJM}\eta_{TM_T}\}. \tag{6}$$

Here $\mathcal{A}$ is an antisymmetrizer acting on the identical baryons, $\boldsymbol{x} = (\boldsymbol{x}_1, \cdots, \boldsymbol{x}_{A-1})$ stands for a set of relative (e.g., Jacobi) coordinates, and χ_{kSM_S} (η_{TM_T}) is the spin (isospin) function of the system. The CG, $G(\boldsymbol{x}, A_k)$, is defined by

$$\begin{aligned} G(\boldsymbol{x}, A_k) &= \exp\Big\{ -\sum_{i<j}^{A} \alpha_{k\,ij} (\boldsymbol{r}_i - \boldsymbol{r}_j)^2 \Big\} \\ &= \exp\Big\{ -\frac{1}{2} \sum_{i,j=1}^{A-1} A_{k\,ij}\, \boldsymbol{x}_i \cdot \boldsymbol{x}_j \Big\}. \end{aligned} \tag{7}$$

The $(A-1)\times(A-1)$ symmetric matrix A_k contains $A(A-1)/2$ independent matrix elements which serve as nonlinear parameters to characterize the CG basis. Since $\boldsymbol{r}_i - \boldsymbol{r}_j$ can be expressed as a combination of $\boldsymbol{x}_m$, $(\boldsymbol{r}_i - \boldsymbol{r}_j)^2$ becomes a combination of quadratic terms $\boldsymbol{x}_m \cdot \boldsymbol{x}_n$, so the two expressions in Eq. (7) are equivalent. The nonlinear parameters $A_{k\,mn}$ can be uniquely expressed in terms of $\alpha_{k\,ij}$ and *vice versa*. The parameters $\alpha_{k\,ij}$ of the former expression are more direct in representing the range of the correlation between the constituent particles [14,27,28].

The trial function (5) has clearly the total orbital angular momentum $L=0$. We assume that the hypernuclei treated in the present study are well described by only $L=0$ component. It is noted, however, that the partial waves corresponding to the coordinate $\boldsymbol{x}_i$ are not restricted to l_i=0, but in general include higher orbital angular momenta [29,30]. This is apparent because the basis function (7) contains the cross terms $\boldsymbol{x}_i \cdot \boldsymbol{x}_j$ in the exponent of the CG and the expansion of those terms into polynomials contains high orbital angular momenta.

The suffix k in χ_{kSM_S} is used to distinguish possible independent spin functions for a given S value [13,14]. For example, in the case where four particles have the total spin S=0, two independent spin functions are possible. We took into account this possibility in the calculation. As for the isospin part we used an appropriately coupled function η_{TM_T} for a given T value.

The set of linear variational parameters $\boldsymbol{c}$=$(c_1, \cdots, c_K)$ of Eq. (5) and the energy E are determined by Ritz variational principle, which leads to the generalized algebraic eigenvalue problem

$$\mathcal{H}\mathbf{c} = E\mathcal{N}\mathbf{c}, \tag{8}$$

where $\mathcal{H}$ and $\mathcal{N}$ are the matrices of the Hamiltonian and of the overlap

$$\mathcal{H}_{ij} = \langle\varphi_i|H|\varphi_j\rangle, \quad \text{and} \quad \mathcal{N}_{ij} = \langle\varphi_i|\varphi_j\rangle \quad (i,j = 1, \cdots, K). \tag{9}$$

The matrix elements of the CGs can be calculated analytically for most of important operators. This plays a key role in obtaining a precise solution for few-body systems. Formulas for the necessary matrix elements are given in Refs. [14,27] and [28]. See also the appendix where we show how to obtain the matrix element for many-particle density operators.

C. Stochastic Variational Method

The basis function φ_k depends on $A(A-1)/2$ nonlinear parameters $\alpha_{k_{ij}}$ or $A_{k_{ij}}$ and also a discrete parameter to specify the intermediate spin quantum numbers in the case when a number of independent spin functions, g, is $g > 1$ for a given S value. These parameters define the shape of the basis function and determine how well the variational function space contains the true eigenfunction. To find the best possible solution, one has to optimize the parameters. By assuming that we need a linear combination of K functions, we face an optimization problem of $K(A(A-1)/2+\epsilon)$ parameters, where ϵ is 0 when $g=1$, or 1 otherwise. The number of parameters becomes very

large to get reasonably accurate solutions. For example, in the case of ${}^{6}_{\Lambda\Lambda}$He, we need $K = 200$ roughly and then end up with 3000 parameters. Moreover, Eq. (8) must be solved to calculate the energy, so that the optimization of the parameters is extremely hard in problems of the present type.

Another serious problem of the minimization of a function is the omnipresence of local minima. A local minimum is the point where the function reaches a minimum in a finite interval of variables and the number of such minima tends to increase exponentially with the size of the problem. The conventional deterministic optimization algorithms (like the Powell or the conjugate gradient method) [31] tend to converge to whichever local minimum they first encounter. To avoid such problems we use the SVM strategy. A key of the SVM is a one by one increase of the basis size by searching the best among many random trials for the basis function.

The SVM strategy we have used here consists of two procedures, *step-by-step* and *refinement* [13,14,32]. The first stage is the following trial and error procedure to increase the basis dimension: Let us assume that the sets $A_1, \cdots, A_{k-1}$ and $g_1, \cdots, g_{k-1}$ have already been selected, and the $(k-1)$-dimensional eigenvalue problem has already been solved. Here the index g_i specifies which spin function is chosen for φ_i from among the g spin functions. The next step is the following:

step-by-step

1. Different sets $(A_k^1, \cdots, A_k^n)$ are generated randomly.

2-1. For each set A_k^i, the g eigenvalue problems of k-dimension are solved with the g different spin functions and the corresponding energies $(E_k^{i1}, \cdots, E_k^{ig})$ are determined.

2-2. The parameter of the spin function that produces the lowest energy E_k^i among the set $(E_k^{i1}, \cdots, E_k^{ig})$ is selected to be g_k^i for the set A_k^i.

3. By repeating the above processes 2-1 and 2-2 from i=1 to n, the energies $(E_k^1, \cdots, E_k^n)$ are determined.

4. The parameter set A_k^m and g_k^m that produces the lowest energy among the set $(E_k^1, \cdots, E_k^n)$ is selected to be the kth parameter set for φ_k.

5. Increase k to $k+1$ and cycle the processes $1-5$.

The essential reason motivating this strategy is the need to sample different parameter sets as fast as possible. The advantage of this procedure is that it is not necessary to recompute the whole Hamiltonian matrix nor is it necessary to perform a new diagonalization at each time when a new parameter is generated [14]. This competitive selection substantially improves the convergence.

Obviously the basis size cannot be increased forever. Moreover, when the kth basis state is selected, the previous states are kept fixed, that is we tried to find the optimal state with respect to previously selected basis states, but actually some of the basis states selected earlier might not be so important anymore because the succeeding states took over their roles. So one may include a refining procedure where the previous states are probed again as described in the following:

refinement

1. Random parameter sets $(A_k^1, \cdots, A_k^n)$ are newly generated.

2. The parameters of the kth basis state are replaced by the new candidates and the energies $(E_K^1, \cdots, E_K^n)$ are calculated.

3. If the best of the new energies is better than the original one, then replace the old parameters with the new ones, otherwise keep the original ones.

4. Cycle this procedure through the basis states from $k = 1$ to K.

The selection of the spin function has to be performed in the step 2 in exactly the same way as in the step-by-step case. One may repeat the refining process till no further significant improvement is obtained. The refinement is useful for suppressing the basis size.

In most of the calculations, we took n as $n \sim 50 \times (A(A-1)/2)$ and generated the matrix A_k by changing $\alpha_{k_{ij}}$ $(i < j, i = 1, \cdots, A-1)$ one by one randomly in the interval listed in Table III, where, by expressing α as

$$\alpha = \frac{1}{d^2}, \tag{10}$$

d was chosen in the range of $[0,\, d_{max}]$. Also listed in the table are values of g used in the present calculation. We show the convergence of the energy for ${}^{5}_{\Lambda\Lambda}$He in Fig. 6. Both procedures of SVM are found to be very effective for obtaining solutions with high quality.

A virial ratio η is often used to test the accuracy of the solution Ψ. According to the virial theorem, the ratio

$$\eta = \left| \frac{\langle \Psi | W | \Psi \rangle}{2 \langle \Psi | T | \Psi \rangle} - 1 \right|, \quad \text{with} \quad W = \sum_{i=1}^{A} \boldsymbol{r}_i \cdot \frac{\partial V}{\partial \boldsymbol{r}_i} \tag{11}$$

must vanish for the eigenstate Ψ of the Hamiltonian [14]. We will calculate η to check the accuracy of our variational solution. Note that a spherical symmetric potential $V(|\boldsymbol{r}_i - \boldsymbol{r}_j|)$ is changed into $rV'(r)$ with $r = |\boldsymbol{r}_i - \boldsymbol{r}_j|$ by the operation of $\sum_{i=1}^{A} \boldsymbol{r}_i \cdot \frac{\partial}{\partial \boldsymbol{r}_i}$.

III. RESULTS

First we show in Table IV the root-mean square (rms) distances of the particles in the Λ- and ΛΛ-hypernuclei together with the typical dimension size K and the virial ratio η. Here the rms distances are defined as follows:

$$\langle r^2 \rangle = \frac{1}{A} \Big\langle \Psi \Big| \sum_{i=1}^{A} (\boldsymbol{r}_i - \boldsymbol{x}_A)^2 \Big| \Psi \Big\rangle, \qquad \langle r_{ij}^2 \rangle = \big\langle \Psi \big| (\boldsymbol{r}_i - \boldsymbol{r}_j)^2 \big| \Psi \big\rangle, \tag{12}$$

where $\boldsymbol{x}_A$ is the center-of-mass coordinate of the system. We see that both ${}^{3}_{\Lambda}$H and ${}^{4}_{\Lambda\Lambda}$H, among others, have very large rms values, reflecting the very small binding energies, as shown below. The rms distance of NN decreases by adding more Λ particles: By adding Λ to ^{2}H, the $\sqrt{\langle r_{NN}^2 \rangle}$ value changes from 3.9 to 3.6 (${}^{3}_{\Lambda}$H) and 3.3 fm (${}^{4}_{\Lambda\Lambda}$H), respectively. A similar but slightly mild change is seen in ^{3}H and ^{3}He as well. In the case of ^{4}He, however, we see that the rms distance of NN hardly changes by the addition of Λ. Generally speaking, the basis size K needed for an accurate solution increases with an increasing number of particles and also with an increasing spatial extension of the system. Comparing the solutions for the different potentials, the potential with an exceedingly large repulsion like the set C or the OBE-sim potential makes an accurate solution more challenging. It is worthwhile noting that the increase of the basis size is rather gentle on these conditions, so that the solutions have been obtained in the order of $\eta \leq 10^{-4}$ in most cases.

A. Λ-Hypernuclei

Table V shows the results of calculation for the Λ-hypernuclei. Since the parameters in Table II are determined to fit the binding energies of the A=3, 4 Λ-hypernuclei, it is apparent that the energies of those nuclei are in good agreement with the experimental data including the excited states of the A=4 system. As noted in subsect. 2.1, we expect that our effective potential has very reasonable relative strength between ${}^{1}S_0$ and ${}^{3}S_1$ states.

Though the potentials of set A and set C are quite different in the shape, they are constructed to be phase equivalent, and the binding energies predicted by these potentials are almost the same. It is an agreeable feature that the phase equivalent potentials predict the same energies for all the nuclei. This is a strong point of the present calculation with high precision. Of course the solution for the case of set C potential requires a larger basis dimension than the one for the case of set A potential, so that the variational solution must be obtained to an accuracy of a few tens of keV regardless of the characteristics of potentials. We note that the above nice feature is not preserved in a naive calculation such as a *frozen core nucleus*+Λ model and that you may draw an erroneous conclusion based on such calculations. For example, if we describe ${}^{5}_{\Lambda}$He as an $\alpha+\Lambda$ model where the α-particle wave function is given by a fixed $(0s)^4$ Slater determinant with the size parameter of 1.39 fm, we obtain quite different $B_\Lambda({}^{5}_{\Lambda}\mathrm{He})$ values depending on the core height of the ΛN potential: 3.95 and 2.29 MeV for set A and set B, respectively (no anomaly in $B_\Lambda({}^{5}_{\Lambda}\mathrm{He})$!). Set C potential does not even bind ${}^{5}_{\Lambda}$He. (Here $B_\Lambda({}^{5}_{\Lambda}\mathrm{He})$ is defined by the difference of the energy of the model α-particle (−23.94 MeV) and the total energy of the $\alpha+\Lambda$ model calculation.)

As seen in Fig. 1, our effective potential is more attractive in ${}^{1}S_0$ than in ${}^{3}S_1$. We asked a question of whether this potential is strong enough to bind an excited state of ${}^{3}_{\Lambda}$H with $J^\pi = \frac{3}{2}^+$. The calculation showed that the energy of the system approaches the deuteron energy, that is, the potential accommodates no such a bound state.

It has been known for a long time that the CSB effect of the ΛN interaction is manifestly exhibited in the B_Λ values of the A=4 hypernuclei. The data suggest that the Λp interaction is stronger than the Λn interaction. Though the

ΛN-ΣN coupling or Λ-Σ^0 mixing is expected to play the significant role in the CSB, no conclusive understanding of the mechanism of CSB has been obtained yet. Both potentials of sets A and C are charge symmetric. An extension to a calculation including the CSB effect will be discussed later.

The result for ${}^{5}_{\Lambda}$He confirms the long standing problem, i.e., the potential fitted to the A=3, 4 data overbinds ${}^{5}_{\Lambda}$He by about 2 MeV. We will come back to this anomaly in sect. 4, where the effects of the quark Pauli principle are discussed.

B. $\Lambda\Lambda$-Hypernuclei

Table VI shows the results of the $\Lambda\Lambda$-hypernuclei. The energies calculated with different ΛN potentials are almost the same. We have examined if a lightest system of $A = 3$ forms a bound state, but have not found a stable $N\Lambda\Lambda$ system with the $\Lambda\Lambda$ potential either OBE-sim or FSS-sim. We have then asked a question of whether or not a bound state is formed for $A \geq 4$ system. We have calculated the energies for various spin S and isospin T states: $(S,T) = (0,0)$, $(0,1)$, $(1,0)$ and $(1,1)$ for ${}^{4}_{\Lambda\Lambda}$H, and $(S,T) = (0,1)$ and $(1,1)$ for ${}^{4}_{\Lambda\Lambda}$He or ${}^{4}_{\Lambda\Lambda}$n. We find that a lightest bound state of $\Lambda\Lambda$-hypernuclei is only ${}^{4}_{\Lambda\Lambda}$H with $(S,T) = (1,0)$ in consistency with the conclusion of Ref. [35]. See Table VI. The binding energy is so small that its existence may be strongly subjected to the strength of the $\Lambda\Lambda$ potential. This state has a structure of a deuteron plus $\Lambda\Lambda$ that is coupled to S=0. Results for A=5 $\Lambda\Lambda$-hypernuclei are also listed in Table VI. It is very likely that both ${}^{5}_{\Lambda\Lambda}$H and ${}^{5}_{\Lambda\Lambda}$He are bound. Experimental search for these $\Lambda\Lambda$-hypernuclei and measurements of their binding energies will provide us with valuable information on the $\Lambda\Lambda$ interaction.

The main component of $\Lambda\Lambda$ is the ${}^1S_0$ state for the A=4$-$6 $\Lambda\Lambda$-hypernuclei, so the total angular momentum J of each hypernucleus is equal to that of the core nucleus. The J and T values are $(J,T) = (\frac{1}{2},\frac{1}{2})$ for ${}^{5}_{\Lambda\Lambda}$H and ${}^{5}_{\Lambda\Lambda}$He, and (0,0) for ${}^{6}_{\Lambda\Lambda}$He. The contribution of the ${}^3S_1$ and the ${}^1S_0$ components of the ΛN potential to the potential energy is determined by N_t and N_s values. Using an arithmetic similar to Eq. (2) we obtain N_t=$\frac{3}{2}(A-2)$ and N_s=$\frac{1}{2}(A-2)$. Their ratio is $N_t : N_s = 3 : 1$ for all these $\Lambda\Lambda$-hypernuclei, as in the case of ${}^{5}_{\Lambda}$He.

The energy of $B_{\Lambda\Lambda}({}^{6}_{\Lambda\Lambda}\mathrm{He})$ is again overbound compared to the empirical value, just as in the case of $B_{\Lambda}({}^{5}_{\Lambda}\mathrm{He})$ shown in Table V. The calculated value of $\Delta B_{\Lambda\Lambda}({}^{6}_{\Lambda\Lambda}\mathrm{He})$ is, however, in reasonable agreement with the experimental value of 4.7 ± 0.6 MeV: $\Delta B_{\Lambda\Lambda} = 4.3$ MeV for OBE-sim $\Lambda\Lambda$ potential and 5.2 MeV for FSS-sim $\Lambda\Lambda$ potential. We thus expect that the strength of the $\Lambda\Lambda$ potentials employed in the present study is nearly right. Rather we guess that the same anomaly known in ${}^{5}_{\Lambda}$He appears in ${}^{6}_{\Lambda\Lambda}$He as well.

C. Density Distributions and Correlation Functions

Obviously the density distribution and the correlation function between the particles provide us with more profound information on the structure of the system than just the average distances of the particles. It is also of particular interest to know the extent to which the core nucleus is distorted by adding the Λ particles. For this purpose we define the distribution function of N or Λ by

$$\rho(\boldsymbol{r}) = \langle \Psi \,|\delta(\boldsymbol{r}_i - \boldsymbol{R}_c - \boldsymbol{r})|\, \Psi \rangle, \tag{13}$$

where $\boldsymbol{r}_i$ denotes the position vector of N or Λ, and $\boldsymbol{R}_c$ is the center-of-mass coordinate of the core nucleus. Therefore $\boldsymbol{r}$ is a position vector from the core nucleus. The density defined above is different from the conventional one which is calculated as a function of a position vector measured from the center-of-mass coordinate of the system. The N or Λ density defined here seems more direct to represent the change with the addition of Λ. See the appendix for the method of calculation of the density and the correlation function etc.

Figures $7-9$ show the density distributions of N and Λ when Λ particles are added to the core nucleus of ^{2}H, ^{3}H or ^{4}He, respectively. The set A ΛN and OBE-sim $\Lambda\Lambda$ potentials are used but other choices of the potentials do not change the result very much. As seen from these figures, the density distributions of N and Λ are quite different. The Λ distribution reaches further more outwardly than the N distribution. The systems of ${}^{3}_{\Lambda}$H and ${}^{4}_{\Lambda\Lambda}$H are extremely spread out because the deuteron is weakly bound and in addition these hypernuclei have very small separation energies. The maximum probability of finding Λ occurs at or near the point where the nucleon probability falls to half of its maximum probability. Figure 8 shows that the Λ distribution is considerably different between the ground and excited states of ${}^{4}_{\Lambda}$H and that the core distortion is larger in the ground state than in the excited state. We see that the addition of Λ particles makes the core nucleus shrink and accordingly the Λ density move to the inner region.

The function $C(\boldsymbol{r})$ defined by

$$C(\boldsymbol{r}) = \langle \Psi \left| \delta(\boldsymbol{r}_i - \boldsymbol{r}_j - \boldsymbol{r}) \right| \Psi \rangle \tag{14}$$

gives the information on the correlation of the constituent particles. The correlation function of $\Lambda\Lambda$ is calculated with the set A ΛN and the OBE-sim $\Lambda\Lambda$ potentials and compared in Fig. 10 for the $\Lambda\Lambda$-hypernuclei, ${}^{\ \ 4}_{\Lambda\Lambda}$H, ${}^{\ \ 5}_{\Lambda\Lambda}$H and ${}^{\ \ 6}_{\Lambda\Lambda}$He. It is noted that the correlation function has vanishingly small amplitudes at short distances, as it should because the OBE-sim $\Lambda\Lambda$ potential has a strong central repulsion. Since the CGs have large amplitudes at short distances of the particles, this vanishing of the correlation function indicates that the CG basis is sufficiently flexible to reproduce such characteristics and that the SVM has been practical in selecting suitable basis sets. The behavior of the correlation function reflects the $\Delta B_{\Lambda\Lambda}$ value defined by Eq. (3): The calculated $\Delta B_{\Lambda\Lambda}$ values are 0.06, 1.2 and 4.3 MeV for ${}^{\ \ 4}_{\Lambda\Lambda}$H, ${}^{\ \ 5}_{\Lambda\Lambda}$H and ${}^{\ \ 6}_{\Lambda\Lambda}$He, respectively. The wider the spatial extension of the correlation function, the weaker the $\Lambda\Lambda$ interaction. We see that the two Λ particles, particularly in ${}^{\ \ 4}_{\Lambda\Lambda}$H, spend almost all the time outside their interaction range. The existence of ${}^{\ \ 4}_{\Lambda\Lambda}$H crucially depends on the strength of the $\Lambda\Lambda$ potential. The peak position of the correlation function moves depending on the size of the underlying core nucleus.

To visualize the structure of the system, it is useful to calculate the two-particle (particularly $\Lambda\Lambda$ of the $\Lambda\Lambda$-hypernuclei) distribution function given by

$$D(\boldsymbol{r}, \boldsymbol{r}') = \langle \Psi \left| \delta(\boldsymbol{r}_i - \boldsymbol{R}_c - \boldsymbol{r}) \delta(\boldsymbol{r}_j - \boldsymbol{R}_c - \boldsymbol{r}') \right| \Psi \rangle. \tag{15}$$

This function depends on the three quantities, r, r' and θ, in the case of $L = 0$ wave function, where θ is the angle between $\boldsymbol{r}$ and $\boldsymbol{r}'$; $\boldsymbol{r} \cdot \boldsymbol{r}' = rr' \cos\theta$. In Fig. 11, the two-$\Lambda$ distribution function $D(\boldsymbol{r}, \boldsymbol{r}')$ weighted by $r^2 r'^2 \sin\theta$ is displayed for ${}^{\ \ 5}_{\Lambda\Lambda}$H. To draw this function we first searched for a point where the probability, $r^2 r'^2 \sin\theta\, D(\boldsymbol{r}, \boldsymbol{r}')$, reaches a maximum. The maximum for ${}^{\ \ 5}_{\Lambda\Lambda}$H appears at the point of $r = r'$=1.8 fm and θ=47°. Drawn in Fig. 11 is the distribution of Λ when the other Λ was placed at that point. Though the point determined above may suggest a configuration of an isosceles triangle with side lengths of 1.8, 1.8 and 1.4 fm, the distribution is actually spread out in a wide region, so that the geometry is to be understood rather loose. For example, the rms distance of $\Lambda\Lambda$ is as large as 3.5 fm, much larger than 1.4 fm.

The core nucleus can be distorted by the addition of Λ particles, that is, the nucleus never remains in its ground state in the hypernucleus but may have mixing in of other states. To calculate the probability that the core nucleus remains in its ground state, we define the spectroscopic factor S by

$$S = \sum_{M_c, M_s} \int d\boldsymbol{r} \left\{ g_{M_c M_s}(\boldsymbol{r}) \right\}^2, \tag{16}$$

where the spectroscopic amplitude $g_{M_c M_s}(\boldsymbol{r})$ for the Λ-hypernuclei is given by

$$g_{M_c M_s}(\boldsymbol{r}) = \left\langle \Psi_{J_c M_c T M_T}({}^{A-1}\mathrm{X}) \chi_{\frac{1}{2} M_s}(\Lambda) \delta(\boldsymbol{x}_{A-1} - \boldsymbol{r}) | \Psi_{JMTM_T}({}^{A}_{\Lambda}\mathrm{X}) \right\rangle. \tag{17}$$

Here $\boldsymbol{x}_{A-1} = \boldsymbol{r}_A - \boldsymbol{R}_c$ is the distance vector of Λ from the center-of-mass of the core nucleus ${}^{A-1}$X, and $\Psi_{J_c M_c T M_T}({}^{A-1}\mathrm{X})$ is the ground state wave function of the core nucleus. If no distortion of the core nucleus is present in the hypernucleus, $\sum_{M_c, M_s} \left\{ g_{M_c M_s}(\boldsymbol{r}) \right\}^2$ reduces to the density distribution of Λ that is defined by Eq. (13).

The spectroscopic factor for the $\Lambda\Lambda$-hypernucleus is calculated in a similar way. The spectroscopic amplitude may be defined by

$$g_{M_c}(\boldsymbol{r}, \boldsymbol{r}') = \left\langle \Psi_{J_c M_c T M_T}({}^{A-2}\mathrm{X}) \chi_{00}(\Lambda\Lambda) \delta(\boldsymbol{x}_{A-2} - \boldsymbol{r}) \delta(\boldsymbol{x}_{A-1} - \boldsymbol{r}') | \Psi_{JMTM_T}({}^{\ \ A}_{\Lambda\Lambda}\mathrm{X}) \right\rangle, \tag{18}$$

where $\boldsymbol{x}_{A-2} = \boldsymbol{r}_{A-1} - \boldsymbol{R}_c$ and $\boldsymbol{x}_{A-1} = \boldsymbol{r}_A - \boldsymbol{R}_{c+\Lambda}$ with $\boldsymbol{R}_{c+\Lambda}$ denoting the center-of-mass of the core nucleus and the Λ. Note that the two Λ particles were assumed to be in spin singlet. The spectroscopic factor S is then obtained by $\left\{ g_{M_c}(\boldsymbol{r}, \boldsymbol{r}') \right\}^2$ summed over M_c and integrated over $\boldsymbol{r}$ and $\boldsymbol{r}'$.

Table VII lists the spectroscopic factors calculated for Λ- and $\Lambda\Lambda$-hypernuclei. We confirm, in conformity with the results of Figs. 7 – 9, that adding more Λ particles results in smaller S values, that is, it leads to the larger distortion of the core nucleus, as expected. There is no experimental information on S values but just one theoretical value is available for ${}^{\ \ 3}_{\Lambda}$H. According to Ref. [8] the value is 0.987, which is in very reasonable agreement with the present estimate (0.991) in spite of the use of quite different potentials. The S values of ${}^{\ \ 5}_{\Lambda}$He and ${}^{\ \ 6}_{\Lambda\Lambda}$He are fairly large compared to those of the other nuclei, which may indicate that the ^{4}He core is considerably stable. As already pointed out, however, these results do not necessarily substantiate that the frozen core model is a perfect model even for the light s-shell hypernuclei. A small distortion becomes sometimes crucial for the accurate evaluation of the binding energies.

D. Charge Symmetry Breaking

The experimental data of the A=4 system imply the CSB of the ΛN interaction. The CSB is observed for both the ground and excited states:

$$\Delta B_\Lambda = B_\Lambda({}^4_\Lambda\mathrm{He}) - B_\Lambda({}^4_\Lambda\mathrm{H}) = 0.35 \pm 0.07\mathrm{MeV},$$
$$\Delta B^*_\Lambda = B_\Lambda({}^4_\Lambda\mathrm{He}^*) - B_\Lambda({}^4_\Lambda\mathrm{H}^*) = 0.24 \pm 0.15\mathrm{MeV}. \quad (19)$$

Bodmer and Usmani [36] investigated the CSB phenomenologically. They suggest that the CSB interaction is effectively spin independent, that is, it has no $\boldsymbol{\sigma}_\Lambda \cdot \boldsymbol{\sigma}_N$ dependence. In their argument, however, the ground and excited states were not treated simultaneously. They modified the strength of the ΛN attraction with respect to the ground or excited state, in spite of the fact that the strength of $\boldsymbol{\sigma}_\Lambda \cdot \boldsymbol{\sigma}_N$ interaction is different from each other in the case of $J^\pi = 0^+$ and 1^+ states. Dalitz *et al.* [5] studied the CSB effect for both cases of the spin-dependent and spin-independent CSB potentials. However, they focused only on the CSB effect of the ground states of ${}^4_\Lambda$H and ${}^4_\Lambda$He. Since the accuracy of the present calculation is high enough to discuss the CSB, we attempted to determine phenomenologically a ΛN interaction which includes the CSB effect.

We introduce the CSB term in both components of the triplet and singlet ΛN potentials (1) as follows

$$V_{0t} \to V_{0t} - v_t\tau_3, \quad V_{0s} \to V_{0s} - v_s\tau_3, \quad (20)$$

where τ_3 is the third component of the isospin matrices:

$$\tau_3|n\rangle = +|n\rangle, \quad \tau_3|p\rangle = -|p\rangle. \quad (21)$$

The modification (20) of the strength implies the CSB potential of the form

$$V_{\mathrm{CSB}} = \left\{\frac{1}{4}(3v_t + v_s)\tau_3 + \frac{1}{4}(v_t - v_s)(\boldsymbol{\sigma}_\Lambda \cdot \boldsymbol{\sigma}_N)\tau_3\right\} \mathrm{e}^{-\kappa r^2}. \quad (22)$$

(Here κ_t and κ_s are assumed to be the same to simplify the expression but no such an assumption was made in the calculation.) If v_t and v_s have the same sign, the spin dependence of the CSB potential becomes weak.

Starting from the set A ΛN potential in Table II, we determined those v_t and v_s values of the CSB potential which reproduce the data as suggested in Eq. (19). For this purpose we examined the energy dependence of the A=4 hypernuclei on the set of v_t and v_s values around (v_t, v_s)=(0, 0). After repeating calculations for different sets of parameters, we found a set of values which reproduces both ΔB_Λ and ΔB^*_Λ very well:

$$v_t = 3.30 \text{ MeV} \quad \text{and} \quad v_s = 2.65 \text{ MeV}. \quad (23)$$

Both v_t and v_s values are positive in sign, so that the CSB potential determined above is weakly spin-dependent in accordance with the conclusion of Ref. [36]. With this CSB potential the Λp phase shifts in ${}^1S_0$ and ${}^3S_1$ states increase to 34 and 21 degrees, respectively.

As listed in Table V, the calculated binding energies with this CSB potential are in good agreement with experimental data. The change of $B_{\Lambda\Lambda}$ with the CSB potential is listed in Table VI. The CSB does not alter the prediction for possible existence of ${}^{\ 5}_{\Lambda\Lambda}$H and ${}^{\ 5}_{\Lambda\Lambda}$He.

The CSB potential produces a very minor change in energy for those hypernuclei which include the same number of protons and neutrons such as ${}^3_\Lambda$H, ${}^{\ 4}_{\Lambda\Lambda}$H, ${}^5_\Lambda$He and ${}^{\ 6}_{\Lambda\Lambda}$He.

The scattering parameters calculated with the CSB potential (23) are compared in Table VIII to predictions by different models. Some models by e.g. Nijmegen group [3,9,10,37] give a spin-dependent CSB interaction and predict the strengths of the ΛN attraction in the order of

$$|a_s^{\Lambda n}| > |a_s^{\Lambda p}| > |a_t^{\Lambda p}| > |a_t^{\Lambda n}|. \quad (24)$$

On the contrary, our potential predicts the opposite order in the ${}^1S_0$ part: As expected, the Λp interaction becomes more attractive than the Λn interaction. In the case of ${}^3S_1$ both the Nijmegen and our phenomenological potentials predict that the Λp interaction is more attractive than the Λn interaction. It is noted that the introduction of the CSB determined in this study improves a fit to the Λp total cross section as displayed in Fig. 4.

IV. QUARK PAULI EFFECT

A. Pauli-forbidden Configuration

As shown in the previous section, the calculated Λ separation energy of ${}^{5}_{\Lambda}$He is overbound by about 2 MeV, compared to experiment. The $\Lambda\Lambda$ separation energy of ${}^{6}_{\Lambda\Lambda}$He is found to be also largely overbound. To resolve these discrepancies is one of the most challenging problems in s-shell hypernuclei. Shinmura *et al.* [7] argued that the noncentral components of the ΛN and NN potentials plays an important role. The effect of the Λ-Σ conversion may become important, as shown by Miyagawa *et al.* [8], through the ${}^3S$-${}^3D$ tensor coupling in the ΛN-ΣN channel. An *ab initio* calculation using realistic potentials has not been performed until now because of the complexity of the potentials. Even if it has been done in some way, there is so large uncertainty in the realistic potentials that such a calculation may not give a perfect answer. The premise we are taking in this study is that the effects of the noncentral forces and the Λ-Σ conversion etc. are renormalized in the effective potential which is determined so as to fit the binding energies of the A=3, 4 Λ-hypernuclei. We thus pay attention to other mechanism, a quark Pauli effect, for examining this problem in this section. The quark Pauli effect was considered in Ref. [38] on the basis of the quark shell model where the quarks were allowed to move in the whole hypernucleus. In contrast to this approach, we treat the Pauli effect by confining three quarks inside the baryons. Parts of the results along this line have been reported in Refs. [11] and [12].

So far we have treated the Λ particle as distinguishable from the nucleon N. Therefore all the baryons in ${}^{5}_{\Lambda}$He or ${}^{6}_{\Lambda\Lambda}$He, for example, may occupy a small region at the same time if that configuration is favorable to the energy gain. In the quark model of baryons, however, Λ and N share quarks of the same flavor, and then in a Λ-hypernuclei with $A \geq 5$ there may be an increasing chance that more than six u or d quarks occupy the same orbit as the baryons come close to each other. Of course this chance is forbidden from the quark Pauli principle, so that it should be excluded in a calculation [11,12]. This type of quark Pauli principle should act even in normal nuclei but its effect is taken into account by the Pauli principle for the N. There is no way, however, to take into account the quark Pauli effect in those calculations which do not consider the quark substructure of the baryon. The aim here is to estimate how much the Λ separation energy changes by the mechanism arising from the quark Pauli effect. We perform this estimation by using only those wave functions which are still expressed in terms of the baryon coordinates. The effect to be discussed here is concerned with a specific forbidden configuration, which is a special effect of a more general antisymmetrization effect of the quarks [39].

A specific quark Pauli-forbidden configuration comprising five baryons was considered in Refs. [11] and [12]:

$$\psi_{\rm F}(\boldsymbol{x}) = \left(\frac{\pi b^2}{3}\right)^{-\frac{3}{4}} \exp\left\{-\frac{3}{2b^2}\sum_{i=1}^{5}(\boldsymbol{r}_i - \boldsymbol{R}_5)^2\right\}, \tag{25}$$

where $\boldsymbol{R}_5$ is the center-of-mass coordinate of the five baryons. This configuration was derived by assuming that a baryon is a three-quark system and that the orbital motion of each quark is described by a $(0s)$ harmonic-oscillator function, $\exp\{-\boldsymbol{r}^2/2b^2\}$. The parameter b determines the size of the baryon. If the simple $(0s)^3$ wave function ought to reproduce the charge radius of proton (0.86 fm) [40], then b becomes 0.86 fm. A more reasonable value of b would be slightly smaller than 0.86 fm if other effects such as meson clouds etc. are considered in the charge radius. We will examine the binding energy change in the range of b=0.6−0.86 fm.

Now the trial function must be subjected to remain in the subspace which is orthogonal to the forbidden state, that is, $\langle\psi_{\rm F}|\Psi\rangle = 0$. We thus modify Eq. (5) by

$$\Psi_{JMTM_T} = \sum_{k=1}^{K} c_k \left(\varphi_k - \sum_a \Gamma_a \langle\Gamma_a|\varphi_k\rangle\right), \tag{26}$$

where Γ_a is an orthonormal set which spans the Pauli-forbidden space. In the case of A=5, Γ_a can simply be represented by $\mathcal{A}\{\psi_{\rm F}\chi\eta\}$. For $A \geq 6$, however, the construction of Γ_a is never trivial. The system ${}^{6}_{\Lambda\Lambda}$He, for example, has three types of forbidden states (25) comprising $ppnn\Lambda$, $ppn\Lambda\Lambda$, or $pnn\Lambda\Lambda$ baryons. A method proposed in Ref. [12] enables us to eliminate practically the Pauli-forbidden components. The reader is referred to Ref. [12] for its detail. The basis functions φ_k were newly selected by the SVM. The accuracy of the solution is an essential ingredient in this calculation because the solution must be accurate enough to be sensitive to small components produced by the quark Pauli principle.

B. Hypernuclei with A=5 and 6

Table IX shows the dependence of the Λ separation energy on the baryon size for the A=5, 6 hypernuclei. The case of b=0 is no quark Pauli calculation. The energy change is insignificant for $b \leq 0.6$ fm. As expected, a significant binding energy reduction is found to occur at $b = 0.86$ fm in ${}^{5}_{\Lambda}$He and ${}^{6}_{\Lambda\Lambda}$He, while the reduction is much less in ${}^{5}_{\Lambda\Lambda}$H and ${}^{5}_{\Lambda\Lambda}$He. The energy of ${}^{6}_{\Lambda\Lambda}$He is apparently overbound in no quark Pauli calculation. The elimination of the forbidden states produces a surprisingly large reduction in the binding energy, the order of half a MeV even at b=0.6 fm, which is very favorable to the anomaly problem. These results can be understood from the fact that ${}^{5}_{\Lambda\Lambda}$H and ${}^{5}_{\Lambda\Lambda}$He are spatially more extended than ${}^{5}_{\Lambda}$He and ${}^{6}_{\Lambda\Lambda}$He. (See Table IV and Figs. $7-9$.) Since the b-dependence of the quark Pauli effect is very moderate in ${}^{5}_{\Lambda\Lambda}$H and ${}^{5}_{\Lambda\Lambda}$He, a measurement of their binding energies will be quite useful for the determination of the ΛΛ attraction.

As the forbidden state (25) is a spatially compact configuration, one may conceive that the energy change be dependent on the characteristics of potentials, especially the height of the central repulsion. Table X compares B_Λ and $B_{\Lambda\Lambda}$ values for different sets of the potentials. The variation of the Λ separation energy for the different potentials is very moderate, so we may conclude that the results of these tables indicate the general trend of the quark Pauli effect in light Λ- and ΛΛ-hypernuclei.

To explain the mild dependence on the potentials we derive an approximate expression for the energy change as follows. Let Ψ_0 and E_0 denote the ground state wave function and the energy of no quark Pauli calculation. When the quark Pauli effect is taken into account, the ground state wave function changes and, since the change is expected to be small, the wave function may be approximated as

$$\Psi = \frac{1}{\sqrt{1-\varepsilon^2}}\,(\Psi_0 - \varepsilon\psi_{\rm F}) \qquad \text{with} \qquad \varepsilon = \langle\psi_{\rm F}|\Psi_0\rangle. \tag{27}$$

The energy change is given by

$$E - E_0 = \langle\Psi|H|\Psi\rangle - E_0 \approx \varepsilon^2\langle\psi_{\rm F}|H|\psi_{\rm F}\rangle, \tag{28}$$

where we used $H\Psi_0 = E_0\Psi_0$ and assumed that ε is small and $\langle\psi_{\rm F}|H|\psi_{\rm F}\rangle \gg E_0$. The energy change is approximately estimated by the product of the probability, ε^2, of finding the forbidden component in Ψ_0 and the energy expectation value of the Pauli-forbidden state, $\langle\psi_{\rm F}|H|\psi_{\rm F}\rangle$. We show in Table XI ε^2, $\langle\psi_{\rm F}|H|\psi_{\rm F}\rangle$, and the energy change calculated with the different potentials. In the case of ${}^{5}_{\Lambda}$He, for example, the set A potential with soft central repulsion gives $\varepsilon^2 = 0.00406$, $\langle\psi_{\rm F}|H|\psi_{\rm F}\rangle = 513$ MeV, while the set C potential with very large repulsion gives $\varepsilon^2 = 0.00331$, $\langle\psi_{\rm F}|H|\psi_{\rm F}\rangle = 969$ MeV. We see that these two factors really depend on the potential but their product is rather weakly dependent on the potential, and close to the binding energy change δE. This feature is a basic reason for the mild dependence of the energy change on the potential. A similar result is seen in the case of ${}^{5}_{\Lambda\Lambda}$H, where the OBE-sim or FSS-sim ΛΛ potential produces almost the same energy change though the core height is quite different between the two potentials. It is also interesting to recognize the difference of the energy change between ${}^{5}_{\Lambda}$He and ${}^{5}_{\Lambda\Lambda}$H. Comparing the results calculated with set A and FSS-sim potentials we understand that, though $\langle\psi_{\rm F}|H|\psi_{\rm F}\rangle$ is almost the same in both cases, ε^2 is significantly different in both nuclei, which explains the larger quark Pauli effect in ${}^{5}_{\Lambda}$He than in ${}^{5}_{\Lambda\Lambda}$H.

V. SUMMARY

We have determined phenomenologically the ΛN central potential so as to reproduce the binding energies of $A = 3$, 4 Λ-hypernuclei on the premise that various effects such as the noncentral forces and the Λ-Σ conversion etc. are renormalized in the effective potential. The phase shifts predicted by this potential reaches 32 and 19 degrees at maximum in ${}^1S_0$ and ${}^3S_1$ states, and the scattering lengths and effective ranges are $a_s = -2.52$ fm, $a_t = -1.20$ fm, $r_s = 3.08$ fm and $r_t = 4.26$ fm, respectively.

Bound state solutions for the Schrödinger equation have been obtained by the stochastic variational method with the correlated Gaussian basis. We have performed a high precision calculation to determine the binding energies of the hypernuclei with $A \leq 6$. We have properly taken into account both the short-range correlation of the particles and the asymptotic behavior of the wave function in setting up the variational trial functions. We have employed the three phase-equivalent ΛN potentials which have different core heights and confirmed that they all give almost the same Λ separation energies for the s-shell Λ-hypernuclei (${}^{3}_{\Lambda}$H, ${}^{4}_{\Lambda}$H, ${}^{4}_{\Lambda}$He, ${}^{4}_{\Lambda}$H*, ${}^{4}_{\Lambda}$He*, ${}^{5}_{\Lambda}$He).

The charge symmetry breaking part of the ΛN potential has been determined so as to reproduce both ΔB_Λ and ΔB^*_Λ values for the $A = 4$ Λ-hypernuclei. We find out that the CSB is weakly spin-dependent in accordance with

the conclusion of Ref. [36]. The Λp potential is more attractive than the Λn one in both ${}^1S_0$ and ${}^3S_1$ states. The Λp phase shifts increase by 2 degrees with the inclusion of the CSB effect. This phenomenology disagrees with the prediction of some OBE models where the CSB is spin-dependent and the Λn potential is more attractive than the Λp potential in ${}^1S_0$ state.

For the study of the $\Lambda\Lambda$-hypernuclei we have used the two different $\Lambda\Lambda$ potentials which reproduce the $\Delta B_{\Lambda\Lambda}({}^{\ 6}_{\Lambda\Lambda}\mathrm{He})$ value reasonably well. The present calculation has shown that we can expect hitherto undiscovered particle-stable $\Lambda\Lambda$-hypernuclei, ${}^{\ 4}_{\Lambda\Lambda}\mathrm{H}$, ${}^{\ 5}_{\Lambda\Lambda}\mathrm{H}$ and ${}^{\ 5}_{\Lambda\Lambda}\mathrm{He}$, with the $B_{\Lambda\Lambda}$ values of 0.4, 5.5 and 6.3 MeV, respectively. No other bound $\Lambda\Lambda$-hypernucleus has been obtained for $A \leq 5$. Since the binding energy of ${}^{\ 4}_{\Lambda\Lambda}\mathrm{H}$ is very small, its existence will crucially depend on the attraction of the $\Lambda\Lambda$ interaction, while both of ${}^{\ 5}_{\Lambda\Lambda}\mathrm{H}$ and ${}^{\ 5}_{\Lambda\Lambda}\mathrm{He}$ are more tightly bound, so that their existence will be very probable. Experimental confirmation of these $\Lambda\Lambda$-hypernuclei will provide us with valuable information on the $\Lambda\Lambda$ interaction.

The structure change produced by adding Λ particles has been investigated by calculating the density distribution, two-particle correlation function and spectroscopic factor etc. The distribution of Λ is in general much broader than that of N. For instance, the root-mean-square distance of the two Λ particles in ${}^{\ 4}_{\Lambda\Lambda}\mathrm{H}$ is larger than 8 fm and they spend almost all the time outside the range of the $\Lambda\Lambda$ interaction.

The present calculation has confirmed the well-known problem that the binding energies of both ${}^{\ 5}_{\Lambda}\mathrm{He}$ and ${}^{\ 6}_{\Lambda\Lambda}\mathrm{He}$ are predicted to be overbound by $2-3$ MeV. We have focused our attention on the effect of the quark substructure of N and Λ to see if the binding energy is reduced by the quark Pauli principle. The effect is negligible if the baryon size in which the quarks are confined is smaller than 0.6 fm, but becomes appreciable, particularly in ${}^{\ 6}_{\Lambda\Lambda}\mathrm{He}$, if the size is taken to be as large as 0.7 fm. To resolve this overbinding problem still remains very challenging and important in few-body hypernuclear systems.

APPENDIX A: MATRIX ELEMENTS OF THE CORRELATED GAUSSIANS

Most of the formulas for the matrix elements of the CG are given elsewhere [14,27–29]. The reader is referred to these references for the detail, so here we recapitulate the basic formulas and the calculation of the correlation function. We consider the system comprising N particles and denote the set of relative coordinates as $(\boldsymbol{x}_1, \cdots, \boldsymbol{x}_{N-1})$.

The CG has two noteworthy advantages in the calculation of matrix elements in addition to its flexibility to represent various shapes of many-variable functions. First the CG does not change its form under the permutation of particle indices. Since the permutation P induces a linear transformation of the coordinates as

$$P\boldsymbol{x}_i = \sum_{j=1}^{N-1} T_{ij}\boldsymbol{x}_j \qquad (i = 1, \cdots, N-1), \tag{A1}$$

we notice that the CG is changed by P into

$$PG(\boldsymbol{x}, A) = G(\boldsymbol{x}, \widetilde{T}AT) \qquad \text{with} \quad \widetilde{T}_{ij} = T_{ji}. \tag{A2}$$

The action of P is thus very simple: The CG remains a new CG with the matrix A being replaced with a new one $\widetilde{T}AT$. Thus the antisymmetry requirement for the basis function involving the CG is relatively easily fulfilled by just knowing the matrix T. We do not need to calculate other matrix elements than those between the CGs. Secondly most of the matrix elements for the CG can be obtained analytically, and this makes it possible to obtain a precise solution with the CG basis.

The overlap of the CG is given by

$$\langle G(\boldsymbol{x}, A)|G(\boldsymbol{x}, A')\rangle = \left(\frac{(2\pi)^{N-1}}{\det B}\right)^{\frac{3}{2}} \qquad \text{with} \quad B = A + A'. \tag{A3}$$

By expressing the kinetic energy operator as

$$\sum_{i=1}^{N} \frac{\boldsymbol{p}_i^2}{2m_i} - T_{cm} = \frac{1}{2}\sum_{i,j=1}^{N-1} \Lambda_{ij}\boldsymbol{\pi}_i \cdot \boldsymbol{\pi}_j \qquad \text{with} \quad \boldsymbol{\pi}_j = -i\hbar\frac{\partial}{\partial \boldsymbol{x}_j}, \tag{A4}$$

we obtain the matrix element for the kinetic energy operator:

$$\langle G(\boldsymbol{x},A)|\sum_{i=1}^{N}\frac{\boldsymbol{p}_i^2}{2m_i}-T_{cm}|G(\boldsymbol{x},A')\rangle$$
$$=\frac{3}{2}\hbar^2\mathrm{Tr}\left(A'B^{-1}A\Lambda\right)\langle G(\boldsymbol{x},A)|G(\boldsymbol{x},A')\rangle. \tag{A5}$$

To calculate the matrix element for the two-body interaction, it is convenient to express the potential in the form

$$V(\boldsymbol{r}_i-\boldsymbol{r}_j)=\int d\boldsymbol{r}V(\boldsymbol{r})\delta(\boldsymbol{r}_i-\boldsymbol{r}_j-\boldsymbol{r}) \tag{A6}$$

and note that the relative distance vector of the particles can be written in terms of the coordinates $\boldsymbol{x}$ as

$$\boldsymbol{r}_i-\boldsymbol{r}_j=\sum_{k=1}^{N-1}\omega_k\boldsymbol{x}_k=\tilde{\omega}\boldsymbol{x}. \tag{A7}$$

Then the matrix element of the potential is given by

$$\langle G(\boldsymbol{x},A)|V(\boldsymbol{r}_i-\boldsymbol{r}_j)|G(\boldsymbol{x},A')\rangle$$
$$=\int d\boldsymbol{r}V(\boldsymbol{r})\langle G(\boldsymbol{x},A)|\delta(\tilde{\omega}\boldsymbol{x}-\boldsymbol{r})|G(\boldsymbol{x},A')\rangle$$
$$=\left(\frac{c}{2\pi}\right)^{\frac{3}{2}}\langle G(\boldsymbol{x},A)|G(\boldsymbol{x},A')\rangle\int d\boldsymbol{r}V(\boldsymbol{r})\exp\left(-\frac{1}{2}cr^2\right), \tag{A8}$$

where

$$\frac{1}{c}=\tilde{\omega}B^{-1}\omega. \tag{A9}$$

To prove this formula, one makes use of the Fourier integral for the δ-function and the many-variable Gauss integration. The advantages of this method are that, since the dependence on the form of the potential appears only through the last integration, different types of potentials can be treated on equal footing and also that the correlation function (14) can already be calculated in the above procedure. By choosing, e.g., $V(\boldsymbol{r})=r^n$ we can get the matrix element of $|\boldsymbol{r}_i-\boldsymbol{r}_j|^n$ very easily.

The calculation of the density distribution of the particle as defined by Eq. (13) poses no problem if one notices that $\boldsymbol{r}_i-\boldsymbol{R}_c$ is expressed in terms of a linear combination of $(\boldsymbol{x}_1,\cdots,\boldsymbol{x}_{N-1})$. One only needs to redefine ω appropriately and then use the formula of Eq. (A8).

By generalizing the method presented above for the matrix element of the δ-function, we can calculate the two-particle distribution function (15) or even more-particle distribution function. All of these functions can be obtained through the following formula:

$$\langle G(\boldsymbol{x},A)|\prod_{i=1}^{n}\delta(\widetilde{w^{(i)}}\boldsymbol{x}-\boldsymbol{\rho}_i)|G(\boldsymbol{x},A')\rangle$$
$$=\left(\frac{\det\mathcal{C}}{(2\pi)^n}\right)^{\frac{3}{2}}\exp\left(-\frac{1}{2}\sum_{i,j=1}^{n}\mathcal{C}_{ij}\boldsymbol{\rho}_i\cdot\boldsymbol{\rho}_j\right)$$
$$\times\langle G(\boldsymbol{x},A)|G(\boldsymbol{x},A')\rangle, \tag{A10}$$

where $\mathcal{C}$ is an $n\times n$ matrix defined by

$$(\mathcal{C}^{-1})_{ij}=\widetilde{w^{(i)}}B^{-1}w^{(j)}. \tag{A11}$$

By integrating the above equation over $\boldsymbol{\rho}_1,\cdots,\boldsymbol{\rho}_n$, one recovers the overlap (A3) of the CG.

FIG. 1. The ${}^1S_0$ (left) and ${}^3S_1$(right) phase shifts of ΛN scattering as a function of Λ momentum p_Λ. Solid lines are obtained by the potentials of sets A, B and C, + by FSS, and $\times$ are by the Nijmegen model F, respectively.

FIG. 2. The ΛN potentials of sets A and C as a function of N-Λ distance r.

FIG. 3. Forward-backward ratio of Λp scattering as a function of Λ momentum p_Λ. Experimental data are taken from Refs. [18] and [19].

FIG. 4. Total cross section of Λp scattering as a function of Λ momentum p_Λ. The dotted line is obtained with the potentials of sets A, B and C, while the solid line is obtained with set A potential including CSB. Experimental data are taken from Refs. [18–21].

FIG. 5. The ${}^1S_0$ phase shifts (left) calculated by the $\Lambda\Lambda$ potentials displayed on the right panel.

FIG. 6. The energy convergence of ${}^{\ }_{\Lambda\Lambda}{}^{5}$He as a function of the basis dimension K. Set A ΛN and FSS-sim $\Lambda\Lambda$ potentials are used. The CSB effect as we discuss in subsect. 3.4 is included. The upper panel is the step-by-step selection up to K=200, and the lower panel shows the refinement at K=200, which is followed by the step-by-step basis extension to K=300 and the second refinement at K=300.

FIG. 7. The density distributions of N and Λ for ^{2}H, ${}^{3}_{\Lambda}$H and ${}^{\ }_{\Lambda\Lambda}{}^{4}$H as a function of r, the distance from the center-of-mass of ^{2}H.

FIG. 8. The density distributions of N and Λ for ^{3}H, ${}^{4}_{\Lambda}$H, ${}^{4}_{\Lambda}$H* and ${}^{\ }_{\Lambda\Lambda}{}^{5}$H as a function of r, the distance from the center-of-mass of ^{3}H.

FIG. 9. The density distributions of N and Λ for ^{4}He, ${}^{5}_{\Lambda}$He and ${}^{\ }_{\Lambda\Lambda}{}^{6}$He as a function of r, the distance from the center-of-mass of ^{4}He.

FIG. 10. The correlation function of two Λ particles for the $\Lambda\Lambda$-hypernuclei, as a function of r, the distance between Λ-Λ.

FIG. 11. The two-Λ distribution function $r^2 r'^2 \sin\theta D(\boldsymbol{r}, \boldsymbol{r}')$ (upper) of ${}^{\ }_{\Lambda\Lambda}{}^{5}$H as a function of r and θ, where $r' = 1.8$ fm and $(x, y) = (r\cos\theta, r\sin\theta)$. The core nucleus ^{3}H is located at the origin and one of the two Λ particles is placed at the point denoted X. The lower panel plots the contour line of the distribution function. Set A ΛN and OBE-sim $\Lambda\Lambda$ potentials are used.

[1] See Nucl. Phys. **A639** (1998) for a review of recent developments.
[2] M. M. Nagels, T. A. Rijken and J. J. de Swart, Phys. Rev. D**15** (1977), 2547.
[3] M. M. Nagels, T. A. Rijken and J. J. de Swart, Phys. Rev. **D20** (1979), 1633.
[4] Y. Fujiwara, C. Nakamoto and Y. Suzuki, Phys. Rev. Lett. **76** (1996), 2242; Phys. Rev. C**54** (1996), 2180 and references therein.
[5] R. H. Dalitz, R. C. Herndon and Y. C. Tang, Nucl. Phys. B**47** (1972), 109.
[6] B. F. Gibson and E. V. Hungerford III, Phys. Rep. **257** (1995), 349.
[7] S. Shinmura, Y. Akaishi and H. Tanaka, Prog. Theor. Phys. **71** (1984), 546.
[8] K. Miyagawa, H. Kamada, W. Glöckle and V. Stoks, Phys. Rev. C**51** (1995), 2905.
[9] P. M. M. Maessen, Th. A. Rijken and J. J. de Swart, Phys. Rev. **C40** (1989), 2226.
[10] Th. A. Rijken, V. G. J. Stokes and Y. Yamamoto, Phys. Rev. **C59** (1999), 21.
V. G. J. Stokes and Th. A. Rijken, *ibid.* **C59** (1999), 3009.
[11] H. Nemura, Y. Suzuki, Y. Fujiwara and C. Nakamoto, Prog. Theor. Phys. **101** (1999), 981.
[12] Y. Suzuki and H. Nemura, Prog. Theor. Phys. **102** (1999), 203.
[13] K. Varga and Y. Suzuki, Phys. Rev. C**52** (1995), 2885.
[14] Y. Suzuki and K. Varga, *Stochastic Variational Approach to Quantum-Mechanical Few-Body Problems*, Lecture Notes in Physics, Vol. m54 (Springer-Verlag, Berlin Heidelberg, 1998).
[15] V. I. Kukulin and V. M. Krasnopol'sky, J. Phys. G: Nucl. Part. Phys. **3** (1977), 795.
[16] D. R. Thompson, M. Lemere and Y. C. Tang, Nucl. Phys. A**286** (1977), 53.
[17] C. Nakamoto, Y. Suzuki and Y. Fujiwara, Prog. Theor. Phys. **94** (1995), 65; *ibid.* **97** (1997), 761.
[18] G. Alexander, U. Karshorn, A. Shapira, G. Yekutieli, R. Engelman, H. Filthuth and W. Lughofer, Phys. Rev. **173** (1968), 1452.
[19] B. Sechi-Zorn, B. Kehoe, J. Twitty and R. A. Burnstein, Phys. Rev. **175** (1968), 1735.
[20] J. A. Kadyk, G. Alexander, J. H. Chan, P. Gaposchkin and G. H. Trilling, Nucl. Phys. **B27** (1971), 13.
[21] J. M. Hauptman, J. A. Kadyk and G. H. Trilling, Nucl. Phys. **B125** (1977), 29.
[22] D. J. Prowse, Phys. Rev. Lett. **17** (1966), 782.
[23] M. Danysz *et al.*, Phys. Rev. Lett. **11** (1963), 29; Nucl. Phys. **49** (1963), 121.
[24] S. Aoki *et al.*, Prog. Theor. Phys. **85** (1991), 1287.
C. B. Dover, D. J. Millener, A. Gal and D. H. Davis, Phys. Rev. **C44** (1991), 1905.
[25] E. Hiyama, M. Kamimura, T. Motoba, T. Yamada and Y. Yamamoto, Prog. Theor. Phys. **97** (1997), 881.
[26] C. Nakamoto, Y. Fujiwara and Y. Suzuki, *Proceedings of the KEK-Tanashi International Symposium on Physics of Hadrons and Nuclei*, *Dec. 14-17, 1998, Tokyo, Japan*, to be published in Nucl. Phys. **A**.
[27] K. Varga and Y. Suzuki, Comp. Phys. Commun. **106** (1997), 157.
[28] J. Usukura, K. Varga and Y. Suzuki, Phys. Rev. A**58** (1998), 1918.
[29] Y. Suzuki, J. Usukura and K. Varga, J. Phys. B: Atomic, Molecular and Optical Physics **31** (1998), 31.
[30] K. Varga, Y. Suzuki and J. Usukura, Few-Body Systems **24** (1998), 81.
[31] W. H. Press, S. A. Teukolsky, W. T. Vetterling and B. P. Flannery, *Numerical Recipes in FORTRAN*, 2nd edition, (Cambridge University Press, New York, 1992).
[32] K. Varga, Y. Ohbayasi and Y. Suzuki, Phys. Lett. B**396** (1997), 1.
[33] M. Jurič *et al.*, Nucl. Phys. **B52** (1973), 1.
[34] M. Bedjidian *et al.*, Phys. Lett. **83B** (1979), 252.
[35] S. Nakaichi-Maeda and Y. Akaishi, Prog. Theor. Phys. **84** (1990), 1025.
[36] A. R. Bodmer and Q. N. Usmani, Phys. Rev. **C31** (1985), 1400.
[37] M. M. Nagels, T. A. Rijken and J. J. de Swart, Ann. Phys. **79** (1973), 338.
[38] E. V. Hungerford and L. C. Biedenharn, Phys. Lett. B**142** (1984), 232.
[39] S. Takeuchi, K. Shimizu and K. Yazaki, Nucl. Phys. **A449** (1986), 617.
S. Takeuchi and K. Shimizu, Phys. Lett. **B179** (1986), 197.
[40] G. G. Simon, Ch. Schmitt, F. Borkowski, and V. H. Walther, Nucl. Phys. A**333** (1980), 381.
M. McCord *et al.*, Nuclear Instruments and Methods in Physics Research B**56/57** (1991), 496.

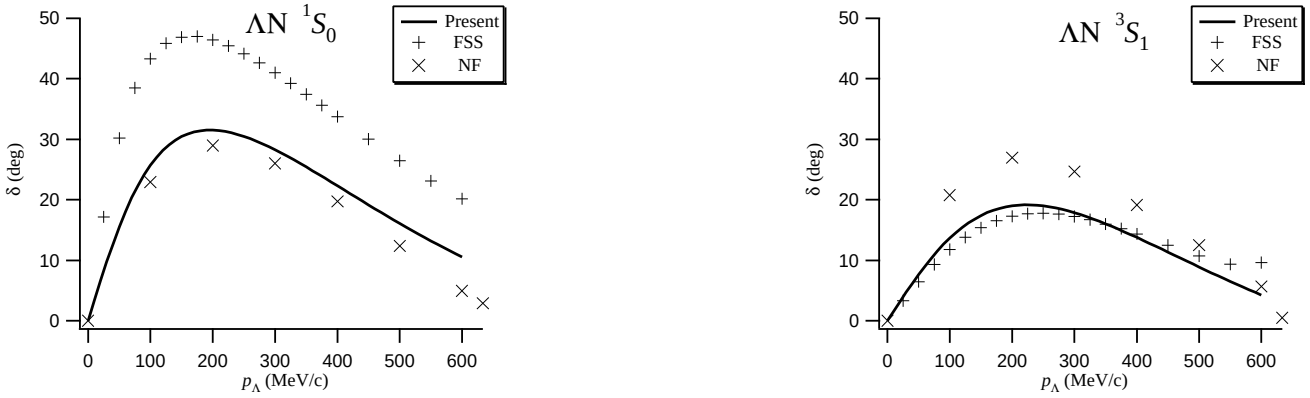
ΛN $^1S_0$
Present
FSS
NF
δ (deg)
p_Λ (MeV/c)
ΛN $^3S_1$
Present
FSS
NF
δ (deg)
p_Λ (MeV/c)

Fig. 1

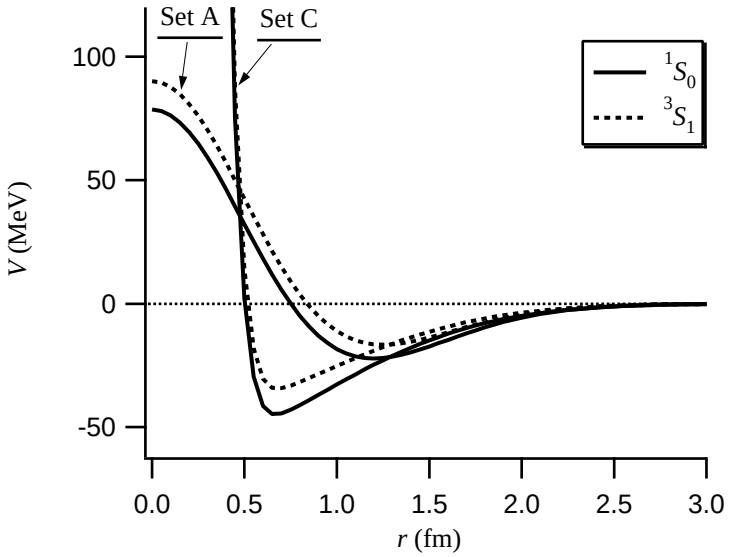
Set A
Set C
$^1S_0$
$^3S_1$
V (MeV)
r (fm)

Fig. 2

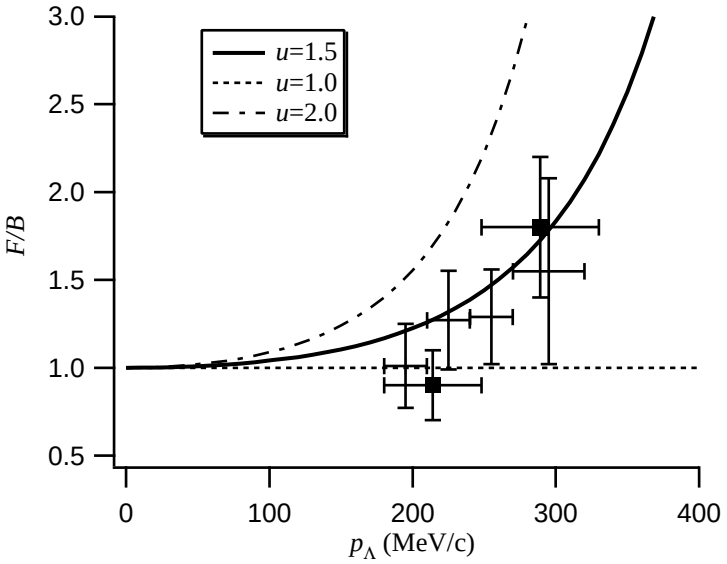
3.0
2.5
2.0
1.5
1.0
0.5
F/B
u=1.5
u=1.0
u=2.0
0
100
200
300
400
p_Λ (MeV/c)

Fig. 3

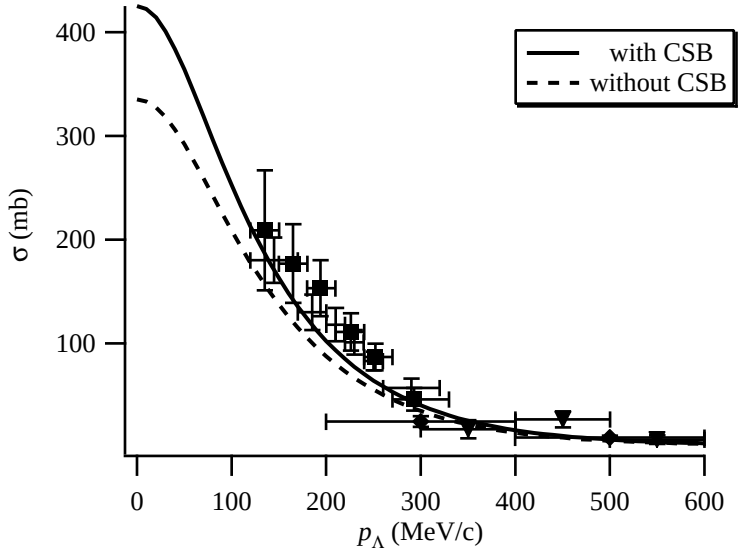
400
300
200
100
σ (mb)
with CSB
without CSB
0
100
200
300
400
500
600
p_Λ (MeV/c)

Fig. 4

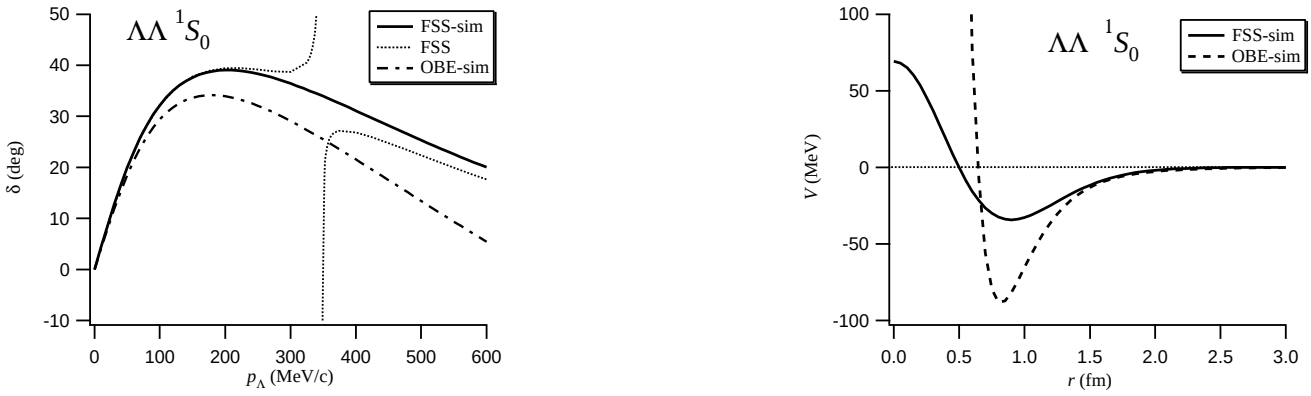
ΛΛ $^1S_0$
FSS-sim
FSS
OBE-sim
δ (deg)
p_Λ (MeV/c)
ΛΛ $^1S_0$
FSS-sim
OBE-sim
V (MeV)
r (fm)

Fig. 5

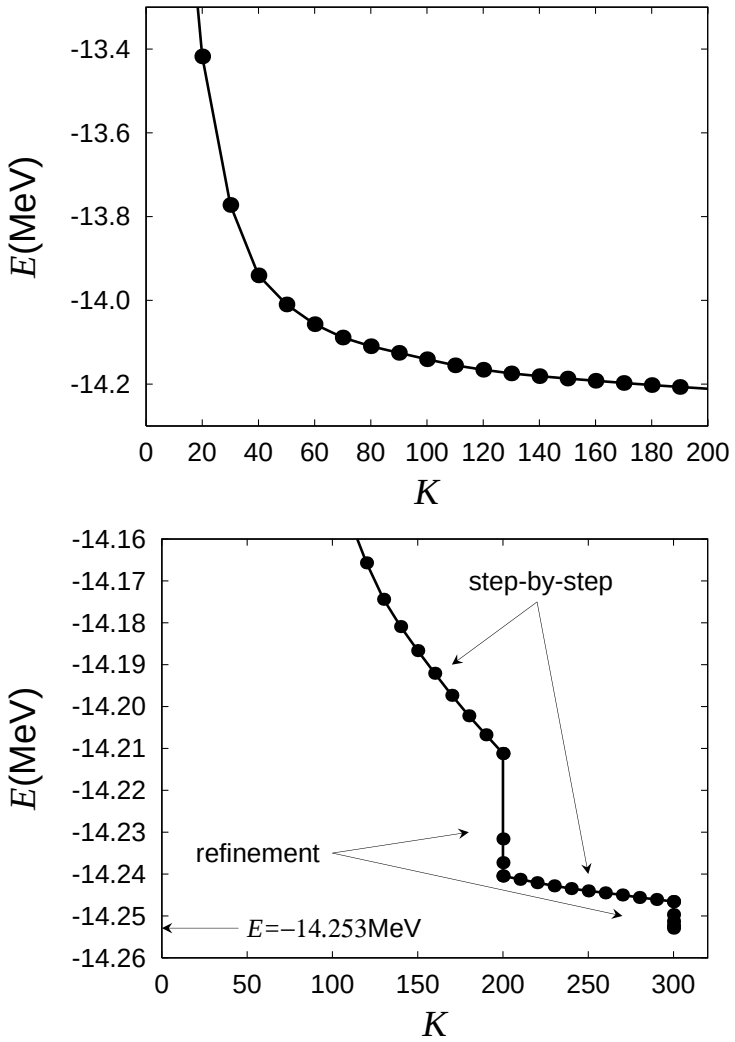
E(MeV)
K
step-by-step
refinement
E=−14.253MeV

Fig. 6

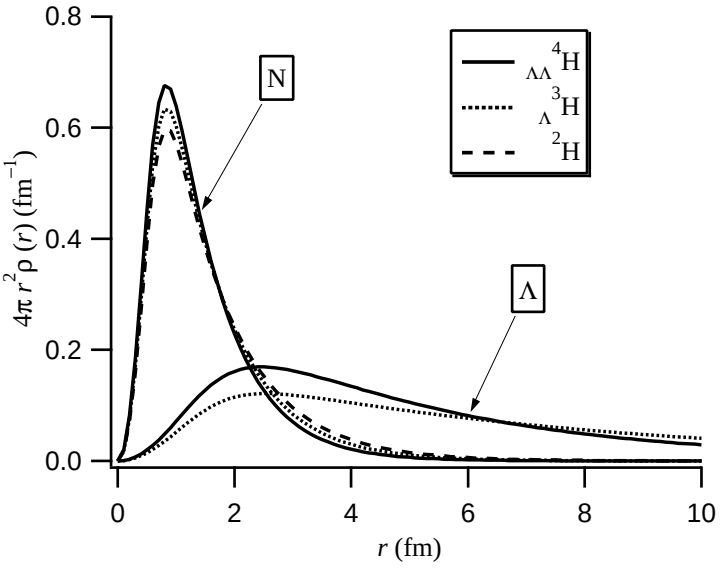
0.8
0.6
0.4
0.2
0.0
0
2
4
6
8
10
$4\pi r^2 \rho(r)$ (fm^{-1})
r (fm)
N
Λ
$^{4}_{\Lambda\Lambda}$H
$^{3}_{\Lambda}$H
^{2}H

Fig. 7

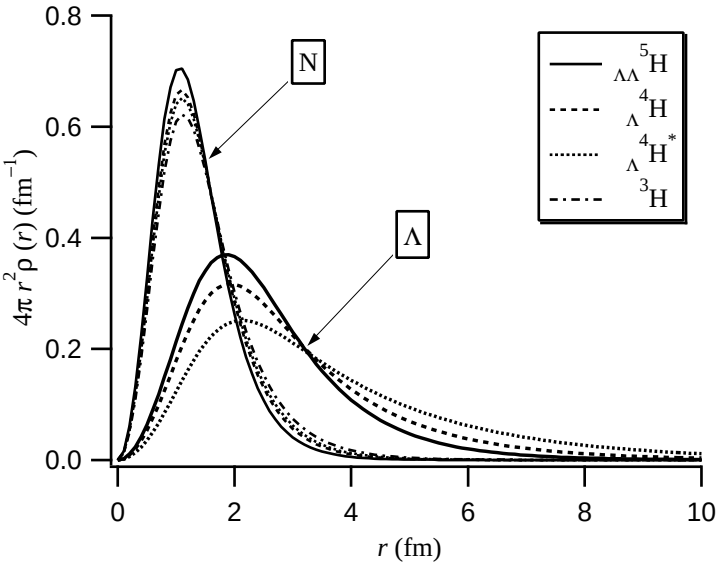
0.8
0.6
0.4
0.2
0.0
0
2
4
6
8
10
$4\pi r^2 \rho(r)$ (fm^{-1})
r (fm)
N
Λ
$^{5}_{\Lambda\Lambda}$H
$^{4}_{\Lambda}$H
$^{4}_{\Lambda}$H*
^{3}H

Fig. 8

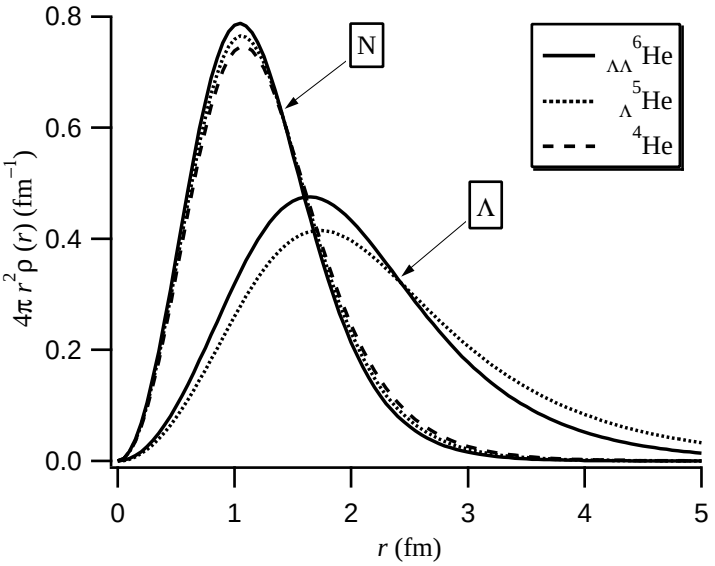
0.8
0.6
0.4
0.2
0.0
0
1
2
3
4
5
$4\pi r^2 \rho(r)$ (fm^{-1})
r (fm)
N
Λ
$_{ΛΛ}^{6}$He
$_{Λ}^{5}$He
^{4}He

Fig. 9

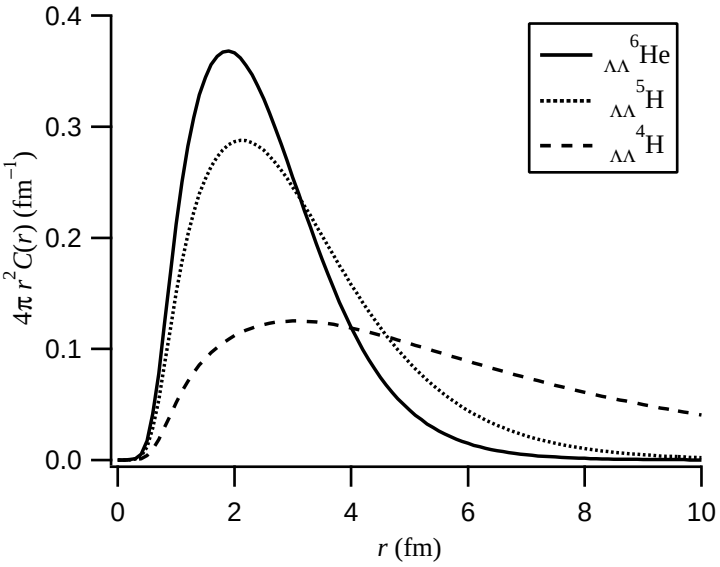
0.4
0.3
0.2
0.1
0.0
0
2
4
6
8
10
$4\pi r^2 C(r)$ (fm^{-1})
r (fm)
$_{ΛΛ}^{6}$He
$_{ΛΛ}^{5}$H
$_{ΛΛ}^{4}$H

Fig. 10

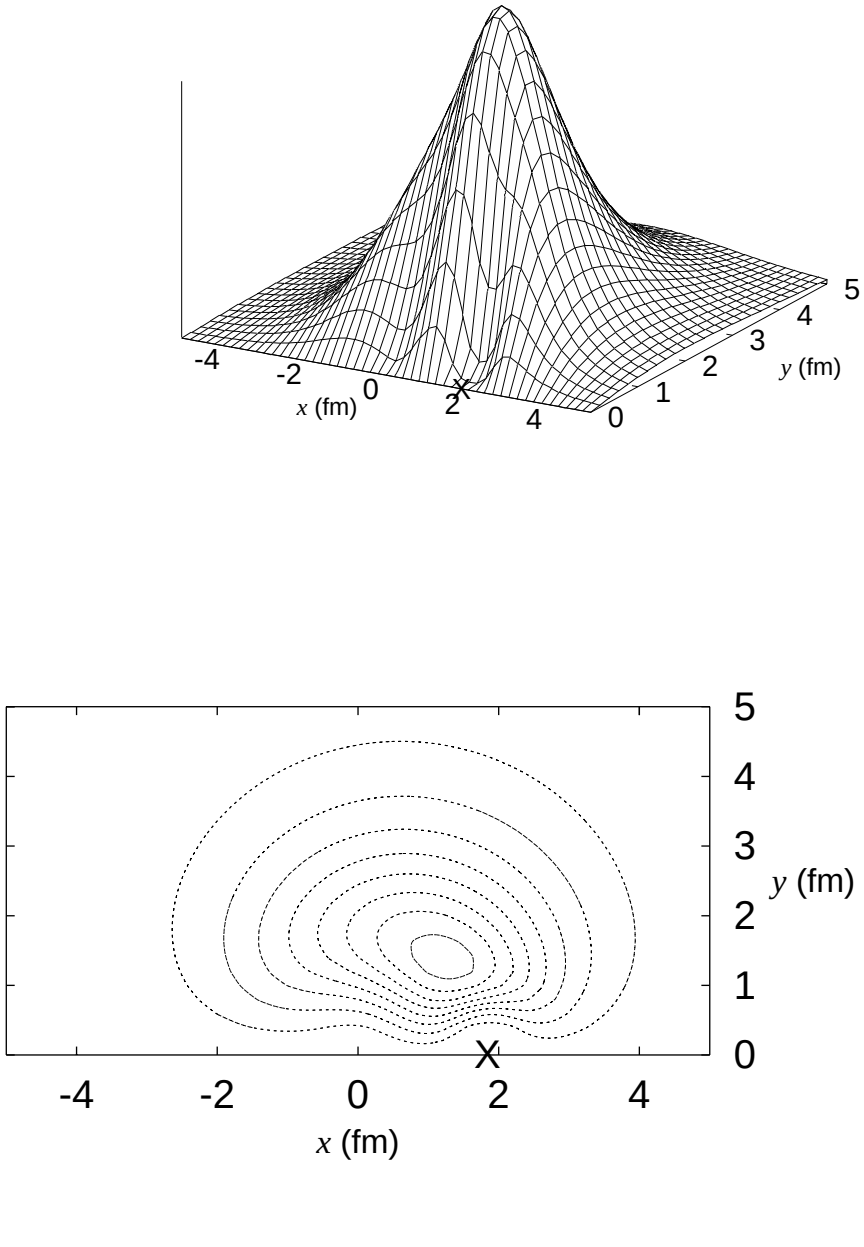

Fig. 11

TABLE I. Contributions of ${}^1S_0$ and ${}^3S_1$ ΛN potentials to the Λ separation energy in a core-nucleus+Λ model. J is the total angular momentum and J_c is the angular momentum of the core nucleus.

	J	J_c	N_s	N_t
${}^3_\Lambda$H	$\frac{1}{2}$	1	$\frac{3}{2}$	$\frac{1}{2}$
	$\frac{3}{2}$	1	0	2
${}^4_\Lambda$H, ${}^4_\Lambda$He	0	$\frac{1}{2}$	$\frac{3}{2}$	$\frac{3}{2}$
	1	$\frac{1}{2}$	$\frac{1}{2}$	$\frac{5}{2}$
${}^5_\Lambda$He	$\frac{1}{2}$	0	1	3

TABLE II. Parameters of NN, ΛN and $\Lambda\Lambda$ potentials. Three sets for the ΛN potential are charge symmetric, giving the same ${}^1S_0$ and ${}^3S_1$ phase shifts in low energy region ($p_\Lambda \leq 600$ MeV/c): The scattering length and effective range are $a_s = -2.52$ fm, $r_s = 3.08$ fm, and $a_t = -1.20$ fm, $r_t = 4.26$ fm. To include the charge symmetry breaking for set A ΛN potential, increase (decrease) both V_{0t} and V_{0s} by the values denoted CSB for Λp (Λn).

		V_{0R} (MeV)	V_{0t} (MeV)	V_{0s} (MeV)	κ_R (fm^{-2})	κ_t (fm^{-2})	κ_s (fm^{-2})
NN	Ref. [16]	200.0	178.0	91.85	1.487	0.639	0.465
ΛN	Set A	200.0	109.8	121.3	1.638	0.7864	0.7513
	CSB$\{^{\Lambda p}_{\Lambda n}\}$		$\{\pm 3.3\}$	$\{\pm 2.7\}$			
	Set B	600.0	52.61	66.22	5.824	0.6582	0.6460
	Set C	5000.0	47.87	61.66	18.04	0.6399	0.6325
$\Lambda\Lambda$	FSS-sim	200.0	–	130.8	2.776	–	1.062

TABLE III. Values of d_{max}, given in units of fm, and the number of spin functions g used in the present calculation. All possible spin functions are taken into account except for ${}_{\Lambda\Lambda}{}^6$He, which is restricted to $[[[S_p, S_p]_0, [S_n, S_n]_0]_0, [S_\Lambda, S_\Lambda]_0]_{00}$.

	d_{max}	g
^{2}H	20	1
^{3}H	15	2
^{3}He	15	2
^{4}He	12	2
${}^3_\Lambda$H	45	2
${}^4_\Lambda$H, ${}^4_\Lambda$He	18	2
${}^4_\Lambda$H*, ${}^4_\Lambda$He*	24	3
${}^5_\Lambda$He	15	5
${}_{\Lambda\Lambda}{}^4$He	55	3
${}_{\Lambda\Lambda}{}^5$H, ${}_{\Lambda\Lambda}{}^5$He	18	5
${}_{\Lambda\Lambda}{}^6$He	15	1

TABLE IV. The root-mean-square distances of Λ- and ΛΛ-hypernuclei. K is the basis dimension and η is the virial ratio defined by Eq. (11). Set A ΛN and OBE-sim $\Lambda\Lambda$ potentials are used.

	$\sqrt{\langle r^2\rangle}$	$\sqrt{\langle r_{NN}^2\rangle}$	$\sqrt{\langle r_{\Lambda N}^2\rangle}$	$\sqrt{\langle r_{\Lambda\Lambda}^2\rangle}$	K	η
^{2}H	1.95	3.90			30	2×10^{-13}
^{3}H	1.71	2.95			30	1×10^{-5}
^{3}He	1.74	3.01			30	1×10^{-4}
					60	6×10^{-6}
^{4}He	1.41	2.30			60	1×10^{-5}
${}^{3}_{\Lambda}$H	4.9	3.6	10.		30	3×10^{-5}
${}^{4}_{\Lambda}$H	2.0	2.7	3.8		100	6×10^{-5}
${}^{4}_{\Lambda}$H*	2.4	2.8	4.7		100	2×10^{-4}
					200	2×10^{-5}
${}^{4}_{\Lambda}$He	2.0	2.8	3.8		100	1×10^{-4}
${}^{4}_{\Lambda}$He*	2.4	2.9	4.8		200	2×10^{-5}
${}^{5}_{\Lambda}$He	1.6	2.3	3.0		200	6×10^{-5}
${}^{4}_{\Lambda\Lambda}$H	4.2	3.3	7.1	8.4	200	5×10^{-4}
${}^{5}_{\Lambda\Lambda}$H	2.0	2.6	3.2	3.5	200	2×10^{-4}
${}^{5}_{\Lambda\Lambda}$He	2.0	2.6	3.3	3.5	200	2×10^{-4}
${}^{6}_{\Lambda\Lambda}$He	1.6	2.2	2.6	2.8	100	2×10^{-4}
					200	8×10^{-5}

TABLE V. Λ separation energies and excitation energies, given in units of MeV, of $A=3-5$ Λ-hypernuclei. *a*) Ref. [33], *b*) Ref. [34].

	$B_\Lambda({}^{3}_{\Lambda}\mathrm{H})$	$B_\Lambda({}^{4}_{\Lambda}\mathrm{H})$	$B_\Lambda({}^{4}_{\Lambda}\mathrm{He})$	$B_\Lambda({}^{5}_{\Lambda}\mathrm{He})$	$E_\mathrm{X}({}^{4}_{\Lambda}\mathrm{H}^{*})$	$E_\mathrm{X}({}^{4}_{\Lambda}\mathrm{He}^{*})$
Set A	0.18	2.24	2.20	4.98	1.14	1.13
with CSB	0.18	2.05	2.40	4.98	1.08	1.19
Set C	0.17	2.21	2.18	4.90	1.13	1.12
Expt.	0.13 ± 0.05^{a}	2.04 ± 0.04^{a}	2.39 ± 0.03^{a}	3.12 ± 0.02^{a}	1.04 ± 0.04^{b}	1.15 ± 0.04^{b}

TABLE VI. ΛΛ separation energies, given in units of MeV, of ΛΛ-hypernuclei. *a*) Ref. [22].

	$B_{\Lambda\Lambda}({}^{4}_{\Lambda\Lambda}\mathrm{H})$	$B_{\Lambda\Lambda}({}^{5}_{\Lambda\Lambda}\mathrm{H})$	$B_{\Lambda\Lambda}({}^{5}_{\Lambda\Lambda}\mathrm{He})$	$B_{\Lambda\Lambda}({}^{6}_{\Lambda\Lambda}\mathrm{He})$
Set A, OBE-sim	0.41	5.6	5.5	14.3
with CSB	0.41	5.2	6.0	14.3
Set A, FSS-sim	0.53	6.1	6.0	15.1
with CSB	0.53	5.7	6.5	15.1
Set C, OBE-sim	0.39	5.5	5.4	13.9
Expt.				10.9 ± 0.6^{a}

TABLE VII. The spectroscopic factors. Set A ΛN and OBE-sim ΛΛ potentials are used.

${}^{3}_{\Lambda}$H	${}^{4}_{\Lambda}$H (0^{+})	${}^{4}_{\Lambda}$H (1^{+})	${}^{5}_{\Lambda}$He	${}^{4}_{\Lambda\Lambda}$H	${}^{5}_{\Lambda\Lambda}$H	${}^{6}_{\Lambda\Lambda}$He
0.991	0.986	0.992	0.994	0.944	0.962	0.985

TABLE VIII. Scattering lengths, in units of fm, predicted by various ΛN interactions including CSB.

	a_s		a_t	
	Λp	Λn	Λp	Λn
Present	-2.83	-2.26	-1.36	-1.06
NSC97f [10]	-2.51	-2.68	-1.75	-1.67
NSC89 [9]	-2.73	-2.86	-1.48	-1.24
NF [3]	-2.18	-2.40	-1.93	-1.84
ND [2]	-1.77 ± 0.28	-2.03 ± 0.32	-2.06 ± 0.12	-1.84 ± 0.10
Ref. [37]	-2.16 ± 0.26	-2.67 ± 0.35	-1.32 ± 0.07	-1.02 ± 0.05
Ref. [5] (with $\boldsymbol{\sigma}_\Lambda \cdot \boldsymbol{\sigma}_N$)	-1.83	-2.45	-1.77	-1.61
Ref. [5] (without $\boldsymbol{\sigma}_\Lambda \cdot \boldsymbol{\sigma}_N$)	-2.45	-1.83	-1.94	-1.47

TABLE IX. Λ and $\Lambda\Lambda$ separation energies, given in units of MeV, of $A = 5$ and 6 hypernuclei as a function of the baryon size b (in fm). The case of $b = 0$ is no quark Pauli calculation. Set A ΛN and OBE-sim $\Lambda\Lambda$ potentials are used. *a*) Ref. [33], *b*) Ref. [22].

	Theory				Expt.
	$b = 0$	0.6	0.7	0.86	
$B_\Lambda({}^{5}_{\Lambda}\mathrm{He})$	4.98	4.90	4.70	3.64	3.12 ± 0.02^a
$B_{\Lambda\Lambda}({}^{5}_{\Lambda\Lambda}\mathrm{H})$	5.6	5.6	5.5	5.1	–
$B_{\Lambda\Lambda}({}^{5}_{\Lambda\Lambda}\mathrm{He})$	5.5	5.5	5.5	5.1	–
$B_{\Lambda\Lambda}({}^{6}_{\Lambda\Lambda}\mathrm{He})$	14.3	13.9	13.0	9.5	10.9 ± 0.6^b

TABLE X. Λ and $\Lambda\Lambda$ separation energies (in MeV) for different potentials. The baryon size is set to $b = 0.86$ fm.

	$B_\Lambda({}^{5}_{\Lambda}\mathrm{He})$	$B_{\Lambda\Lambda}({}^{5}_{\Lambda\Lambda}\mathrm{H})$	$B_{\Lambda\Lambda}({}^{6}_{\Lambda\Lambda}\mathrm{He})$
Set A, OBE-sim	3.64	5.1	9.5
Set C, OBE-sim	3.52	5.0	9.0
Set A, FSS-sim	3.64	5.5	9.9

TABLE XI. The energy change due to quark Pauli effects. The baryon size is set to $b = 0.86$ fm. Energy is given in units of MeV. δE denotes the binding energy change $B_\Lambda(b = 0) - B_\Lambda(b = 0.86)$ for ${}^{5}_{\Lambda}\mathrm{He}$ or $B_{\Lambda\Lambda}(b = 0) - B_{\Lambda\Lambda}(b = 0.86)$ for ${}^{5}_{\Lambda\Lambda}\mathrm{H}$.

		ε^2	$\langle\psi_\mathrm{F}\|H\|\psi_\mathrm{F}\rangle$	$\varepsilon^2\langle\psi_\mathrm{F}\|H\|\psi_\mathrm{F}\rangle$	δE
${}^{5}_{\Lambda}\mathrm{He}$	set A	0.00406	513	2.1	1.34
	set C	0.00331	969	3.2	1.37
${}^{5}_{\Lambda\Lambda}\mathrm{H}$	set A, OBE-sim	0.00117	827	0.97	0.5
	set A, FSS-sim	0.00184	522	0.96	0.6
	set C, OBE-sim	0.000815	1511	1.2	0.5